Solar Phys (2008) 250: 347–374
DOI 10.1007/s11207-008-9221-9

# Expected *in Situ* Velocities from a Hierarchical Model for Expanding Interplanetary Coronal Mass Ejections

**P. Démoulin · M.S. Nakwacki · S. Dasso · C.H. Mandrini**

Received: 21 December 2007 / Accepted: 2 June 2008 / Published online: 8 July 2008


**Abstract** *In situ* data provide only a one-dimensional sample of the plasma velocity along the spacecraft trajectory crossing an interplanetary coronal mass ejection (ICME). Then, to understand the dynamics of ICMEs it is necessary to consider some models to describe it. We derive a series of equations in a hierarchical order, from more general to more specific cases, to provide a general theoretical basis for the interpretation of in situ observations, extending and generalizing previous studies. The main hypothesis is a self-similar expansion, but with the freedom of possible different expansion rates in three orthogonal directions. The most detailed application of the equations is though for a subset of ICMEs, magnetic clouds (MCs), where a magnetic flux rope can be identified. The main conclusions are the following ones. First, we obtain theoretical expressions showing that the observed velocity gradient within an ICME is not a direct characteristic of its expansion, but that it depends also on other physical quantities such as its global velocity and acceleration. The derived equations quantify these dependencies for the three components of the velocity. Second, using three different types of data we show that the global acceleration of ICMEs has, at most, a small contribution to the in situ measurements of the velocity. This eliminates prac-

P. Démoulin (✉)
Observatoire de Paris, LESIA, UMR 8109 (CNRS), 92195 Meudon Principal Cedex, France
e-mail: pascal.demoulin@obspm.fr

M.S. Nakwacki · S. Dasso · C.H. Mandrini
Instituto de Astronomía y Física del Espacio, CONICET-UBA, CC. 67, Suc. 28, 1428 Buenos Aires, Argentina

M.S. Nakwacki
e-mail: sole@iafe.uba.ar

S. Dasso
e-mail: sdasso@iafe.uba.ar

C.H. Mandrini
e-mail: mandrini@iafe.uba.ar

S. Dasso
Departamento de Física, Facultad de Ciencias Exactas y Naturales, Universidad de Buenos Aires, 1428 Buenos Aires, Argentina

tically one contribution to the observed velocity gradient within ICMEs. Third, we provide a method to quantify the expansion rate from velocity data. We apply it to a set of 26 MCs observed by Wind or ACE spacecrafts. They are typical MCs, and their main physical parameters cover the typical range observed in MCs in previous statistical studies. Though the velocity difference between their front and back includes a broad range of values, we find a narrow range for the determined dimensionless expansion rate. This implies that MCs are expanding at a comparable rate, independently of their size or field strength, despite very different magnitudes in their velocity profiles. Furthermore, the equations derived provide a base to further analyze the dynamics of MCs/ICMEs.

**Keywords** Coronal mass ejections, interplanetary · Magnetic fields, interplanetary

## 1. Introduction

Interplanetary coronal mass ejections (ICMEs) are the interplanetary manifestation of magnetized plasma structures ejected from the Sun (*e.g.*, Wimmer-Schweingruber, 2006). ICMEs are dynamic structures moving in the solar wind (SW). The size of an ICME increases during its travel from the Sun to the external heliosphere. Also the bulk velocity of an ICME is usually different from its surrounding solar wind speed since CMEs are launched from the Sun with a large range of speeds. Moreover, ICMEs are accelerated/decelerated as a result of the ICME-SW interaction, *e.g.*, due to drag forces between the ICME and the solar wind environment (*e.g.*, Vršnak and Gopalswamy, 2002).

Magnetic clouds (MCs) are a particular subset of ICMEs (*e.g.*, Burlaga, 1995) that are formed by twisted magnetic flux tubes. The main signatures of a MC are: *i*) an enhanced magnetic field, *ii*) a smooth rotation of the magnetic field vector through a large angle ($\approx 180°$), and *iii*) a low proton temperature (Klein and Burlaga, 1982).

Precise measurements (*in situ*) of magnetic field and plasma properties are available only along the trajectory of the ICME crossing the spacecraft. Then, one needs to rely on a model to derive the global magnetic structure from local measurements. This restricts the analysis to MCs since their magnetic structure is better understood than for the generality of ICMEs. This is most probably because the spacecraft crosses the magnetic configuration closer to its center (Jian *et al.*, 2006).

The most popular magnetic models so far neglect the evolution of the magnetic field during the crossing time of the spacecraft by the observed MC. The magnetic field in MCs is relatively well modeled by the so-called Lundquist model (Lundquist, 1950), which considers a static and axially-symmetric linear force-free magnetic configuration (*e.g.*, Goldstein, 1983; Burlaga, 1988, 1995; Lepping, Burlaga, and Jones, 1990; Lynch *et al.*, 2003). However, many other different models have been also used. Farrugia *et al.* (1999) considered a cylindrical shape for the cloud cross section and a non-linear force-free field, while Mulligan *et al.* (1999), Hidalgo *et al.* (2002), and Cid *et al.* (2002) considered a cylindrical cloud with a finite plasma pressure. Non-cylindrical static models have been also applied to MCs (*e.g.*, Hu and Sonnerup, 2001; Vandas and Romashets, 2002).

MCs usually present a significantly larger velocity in their front than in their back, a characteristic of expansion. Dynamical models have been used to describe these clouds, either considering only a radial expansion (*e.g.*, Farrugia *et al.*, 1993; Osherovich, Farrugia, and Burlaga, 1993; Farrugia, Osherovich, and Burlaga, 1997; Nakwacki *et al.*, 2008), or expansion in both the radial and axial directions (*e.g.*, Shimazu and Vandas, 2002; Berdichevsky, Lepping, and Farrugia, 2003; Dasso *et al.*, 2007). The main aim of these models is to take

into account the evolution of the magnetic field as the MC crosses the spacecraft; then, to correct the effect of mixing spatial-variation/time-evolution in the one-point observations to obtain a better determination of the MC field configuration.

We derive here equations to describe ICMEs and MCs assuming a self-similar expansion. We include an expansion anisotropy, *i.e.*, we allow a different rate in the three main orthogonal directions of the structure. In Section 2, we derive a set of basic equations in a hierarchical way (to be applied from the most general interplanetary structure to the one with specific properties), so that intermediate equations, with less hypotheses, can also be used. The equations describe the expected velocity observed when crossing an expanding structure. This approach then relates the physical characteristics of the expanding structure to the simulated local measurements. Several estimations of the global acceleration of MCs/ICMEs, based in observed cases, are compared in Section 3 in order to estimate the influence of the global acceleration on the observed velocity profile. In Section 4, we determine the expected effects of the expansion and the global acceleration of the structure on simulated measurements of the magnetic field in flux ropes. Then, in Section 5 we present the first application of the theoretical equations developed in Section 2 to observed MCs, and we compare the observed and expected asymmetric magnetic field profiles derived in Section 4. Finally, we give our conclusions in Section 6.

## 2. Equations for an Expanding Structure

In this section we derive the equations for an expanding magnetic structure in the solar wind, such as ICMEs and MCs. We proceed by steps from general to more specific hypotheses.

### 2.1. General Framework

First, we introduce the general framework for the description of ICMEs. This requires four hypotheses, which we shortly justify just after their introduction. We describe the expansion of the magnetic structure with respect of its center located at $\mathbf{r}_c(t)$, where $t$ is the time. The location of a plasma element, with respect to the center, is given by $\mathbf{r}_e(t)$, and from a general reference point, it is given by $\mathbf{r}(t)$, with

$$\mathbf{r}(t) = \mathbf{r}_c(t) + \mathbf{r}_e(t). \tag{1}$$

The time derivative following a given plasma element provides its velocity:

$$\mathbf{v}(t) = \mathbf{v}_c(t) + \mathbf{v}_e(t). \tag{2}$$

**Hypothesis 1** We assume that the global motion of the center, $\mathbf{v}_c$, and the expansion motion, $\mathbf{v}_e$, can be described separately.

This decomposition is justified since different forces are acting to modify the global and internal motions. The global motion is mostly affected by the drag force between the ICME and the solar wind. Moreover, during the spacecraft crossing time, $\mathbf{v}_c$ is approximately constant (Section 3), so Equation (2) is approximately a Galilean transformation. The expansion is mainly driven by internal forces and the decrease with time of the total pressure at the ICME boundary (as the ICME moves away from the Sun). This separation in global and internal motions is only an approximation since a magnetic structure, like an ICME, is a deformable structure. For example, a fast ICME is compressed in the front; so that the internal

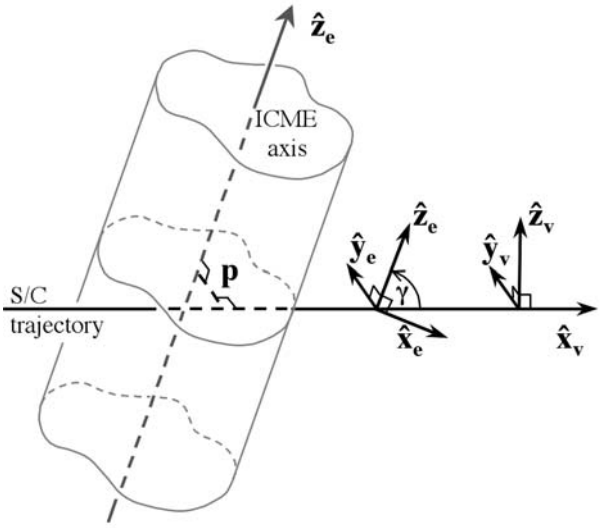


**Figure 1** Geometry and frame vectors associated to the encounter of an ICME with the spacecraft. The three principal axes of expansion are $(\hat{\mathbf{x}}_e, \hat{\mathbf{y}}_e, \hat{\mathbf{z}}_e)$. The configuration is supposed to be locally invariant by translation along $\hat{\mathbf{z}}_e$. The frame $(\hat{\mathbf{x}}_v, \hat{\mathbf{y}}_v, \hat{\mathbf{z}}_v)$ is associated with the global ICME motion, with the velocity of the ICME center along $-\hat{\mathbf{x}}_v$, and with the choice $\hat{\mathbf{y}}_v = \hat{\mathbf{y}}_e$. $p$ is the impact parameter defined by the closest distance between the spacecraft trajectory and the ICME axis.

expansion along the global motion is affected by this interaction. This effect is partly taken into account by introducing an anisotropic expansion.

**Hypothesis 2** The expansion has three principal directions given by the orthonormal vectors $\hat{\mathbf{x}}_e, \hat{\mathbf{y}}_e, \hat{\mathbf{z}}_e$ fixed in time. In each direction there is a self-similar expansion, so that the coordinates of an element of plasma at time $t$ is simply scaled by a time-dependent factor compared to its value at the reference time $t_0$. Then, the position of an element of fluid is described by

$$\mathbf{r}(t) = \mathbf{r}_c(t) + x_e(t)\hat{\mathbf{x}}_e + y_e(t)\hat{\mathbf{y}}_e + z_e(t)\hat{\mathbf{z}}_e \tag{3}$$

$$= \mathbf{r}_c(t) + x_e(t_0)e(t)\hat{\mathbf{x}}_e + y_e(t_0)f(t)\hat{\mathbf{y}}_e + z_e(t_0)g(t)\hat{\mathbf{z}}_e, \tag{4}$$

where $x_e(t), y_e(t), z_e(t)$ are the relative fluid coordinates, with respect to the center, at the time $t$, and where $x_e(t_0), y_e(t_0), z_e(t_0)$ are taken at the fixed time $t_0$.

Previous works have mainly considered an expansion proportional to the time and two particular cases: either only a radial expansion ($e(t) = f(t) \propto t, g(t) = 1$), or an isotropic expansion ($e(t) = f(t) = g(t) \propto t$). These works give the impression that these two expansion modes are the only possible ones. However, there is no physical reason to assume that the expansion should be limited to only one of these two modes. Furthermore, observations show that the evolution of ICME sizes with solar distance, so with time, has a non-linear behavior (typically power laws are used to describe these observations, see Section 2.5). Indeed, the three functions $e(t), f(t), g(t)$ are unknown for individual events, so below we keep them general as long as possible in the hierarchical derivation of the equations. Ideally, observations should constrain them for each observed ICME. However, with present observations, we show that it is not possible; so, we give some reasonable functional dependence for them based on observations from large sets of ICMEs (Section 2.5).

A self-similar expansion requires that the internal evolution can react faster than the evolution imposed at the boundaries, so that the configuration can adjust rapidly enough to be a scaled reproduction of itself at later times. The internal time scale is given by the

Alfven time to cross the structure ($\approx 10$ h for $v_A \approx 400$ km s$^{-1}$ and a size of 0.1 AU), while the time scale of the boundary is given by the pressure evolution of the solar wind as the ICME moves away from the Sun (giving a time scale of $\approx 1$ day). So, the self-similar approximation is expected to be a better approximation for small ICMEs, while it could be a good first approximation for typical ICMEs. A self-similar expansion also requires that the balance of internal forces is not significantly changed during the expansion (for example, the balance between magnetic tension and pressure). The full justification of this hypothesis is left for a future analysis, while it was used in previous works (see, *e.g.*, Chen, 1996).

Deriving Equation (4) with respect to the time, keeping $x_e(t_0)$, $y_e(t_0)$, $z_e(t_0)$ constant to follow the same element of fluid (they are Lagrangian coordinates labeling a given plasma blob), we obtain the fluid velocity:

$$\mathbf{v}(t) = \mathbf{v}_c(t) + x_e(t_0)e'(t)\hat{\mathbf{x}}_e + y_e(t_0)f'(t)\hat{\mathbf{y}}_e + z_e(t_0)g'(t)\hat{\mathbf{z}}_e, \tag{5}$$

where the prime means the time derivative.

The self-similar expansion [Equation (4)] does not define a center for the expansion, *i.e.*, the expansion velocities around each point of the structure are the same. This is easily shown by using Equation (5) for another point, called "b", located at $x_{e,b}(t_0)$, $y_{e,b}(t_0)$, $z_{e,b}(t_0)$:

$$\mathbf{v}_b(t) = \mathbf{v}_c(t) + x_{e,b}(t_0)e'(t)\hat{\mathbf{x}}_e + y_{e,b}(t_0)f'(t)\hat{\mathbf{y}}_e + z_{e,b}(t_0)g'(t)\hat{\mathbf{z}}_e.$$

Subtracting this last equation from Equation (5), we have

$$\mathbf{v}(t) = \mathbf{v}_b(t) + (x_e - x_{e,b})e'(t)\hat{\mathbf{x}}_e + (y_e - y_{e,b})f'(t)\hat{\mathbf{y}}_e + (z_e - z_{e,b})g'(t)\hat{\mathbf{z}}_e,$$

where we have omitted writing the $t_0$ dependence. This last equation has exactly the same form as Equation (5), but now the origin of the spatial coordinates to describe the expansion is located at point b. Then, the center of the ICME is rather selected so that Hypothesis 1 is best satisfied. Using the center of mass is the most natural choice since its velocity is only determined by the sum of the external forces. In practice, the center of the magnetic configuration is usually taken since it can be determined from modeling the magnetic data (while the spatial distribution of density is not available). This is also a natural choice since the magnetic forces are expected to drive the internal expansion, defining the magnetic center as the expected center of expansion.

**Hypothesis 3** The observations by the spacecraft are done at a fixed spatial position, noted $\mathbf{r}_{sc}$.

This is justified since the spacecraft position changes only slightly during the ICME crossing, especially for observations at L1 (*e.g.*, from spacecraft ACE/Wind) where the change is $< 10^{-4}$ AU compared to the size of the observed ICMEs ($\approx 10^{-2}$ to $10^{-1}$ AU). For other spacecrafts, like Ulysses, the change can reach $\approx 10^{-2}$ AU (compared to the ICME sizes of a few $10^{-1}$ AU). If the precision of this approximation is not enough, then it can be replaced by the knowledge of the spacecraft trajectory, $\mathbf{r}_{sc}(t)$. From Equation (4) and $\mathbf{r}(t) = \mathbf{r}_{sc}$, we can eliminate the unknown fluid position $x_e(t_0)$, $y_e(t_0)$, $z_e(t_0)$ in Equation (5), which rewrites as

$$\begin{aligned}\mathbf{v}(t) = \mathbf{v}_c(t) &+ \left[\mathbf{r}_{sc} - \mathbf{r}_c(t)\right] \cdot \hat{\mathbf{x}}_e \frac{e'(t)}{e(t)}\hat{\mathbf{x}}_e \\ &+ \left[\mathbf{r}_{sc} - \mathbf{r}_c(t)\right] \cdot \hat{\mathbf{y}}_e \frac{f'(t)}{f(t)}\hat{\mathbf{y}}_e \\ &+ \left[\mathbf{r}_{sc} - \mathbf{r}_c(t)\right] \cdot \hat{\mathbf{z}}_e \frac{g'(t)}{g(t)}\hat{\mathbf{z}}_e.\end{aligned} \tag{6}$$

**Hypothesis 4** The motion of the ICME center is rectilinear during the crossing time. The rectilinear trajectory of the ICME center is set along the fixed unit vector, called $\hat{\mathbf{x}}_\mathrm{v}$.

Deviations from a radial motion are observed in some cases of CMEs in the low corona (within the field of view of the coronagraph C2 of LASCO onboard SOHO), but not at larger distances (within the field of view of the coronagraph C3). The trajectory deviation is usually interpreted as the interaction between the CME and a nearby streamer (Gopalswamy, Hanaoka, and Hudson, 2000; Bemporad *et al.*, 2005). The interaction with the solar wind, at larger distances, is not expected to give significant deviations of the trajectory, at least on the time scale of the crossing. This will be directly tested by the heliospheric imagers onboard STEREO spacecrafts.

We set $\hat{\mathbf{x}}_\mathrm{v}$ in the opposite direction to the center velocity, $\hat{\mathbf{x}}_\mathrm{v} = -\mathbf{v}_\mathrm{c}/v_\mathrm{c}$, so that $\hat{\mathbf{x}}_\mathrm{v}$ is in practice close to $\hat{\mathbf{x}}_\mathrm{GSE}$, where GSE are the Geocentric Solar Ecliptic coordinates, with $\hat{\mathbf{x}}_\mathrm{GSE}$ pointing towards the Sun, $\hat{\mathbf{z}}_\mathrm{GSE}$ pointing towards the ecliptic north, and $\hat{\mathbf{y}}_\mathrm{GSE}$ such that ($\hat{\mathbf{x}}_\mathrm{GSE}$, $\hat{\mathbf{y}}_\mathrm{GSE}$, $\hat{\mathbf{z}}_\mathrm{GSE}$) is a right handed system. Let us define $\mathbf{p}$ as the vector going from the ICME center to the spacecraft, with $|\mathbf{p}|$ being the closest approach between them, then

$$\mathbf{p} \cdot \hat{\mathbf{x}}_\mathrm{v} = 0. \tag{7}$$

Any rectilinear motion of the ICME center from the spacecraft can be written as

$$\mathbf{r}_\mathrm{c}(t) = \mathbf{r}_\mathrm{sc} - \mathbf{p} + h(t)\hat{\mathbf{x}}_\mathrm{v}, \tag{8}$$

where $h(t_\mathrm{c}) = 0$ with $t_\mathrm{c}$ being the time of the closest approach (between the spacecraft and the ICME center).

With Equation (8), Equation (6) is rewritten as

$$\begin{aligned}\mathbf{v}(t) = {} & h'(t)\hat{\mathbf{x}}_\mathrm{v} + \left[\mathbf{p} - h(t)\hat{\mathbf{x}}_\mathrm{v}\right] \cdot \hat{\mathbf{x}}_\mathrm{e} \frac{e'(t)}{e(t)} \hat{\mathbf{x}}_\mathrm{e} \\ & + \left[\mathbf{p} - h(t)\hat{\mathbf{x}}_\mathrm{v}\right] \cdot \hat{\mathbf{y}}_\mathrm{e} \frac{f'(t)}{f(t)} \hat{\mathbf{y}}_\mathrm{e} \\ & + \left[\mathbf{p} - h(t)\hat{\mathbf{x}}_\mathrm{v}\right] \cdot \hat{\mathbf{z}}_\mathrm{e} \frac{g'(t)}{g(t)} \hat{\mathbf{z}}_\mathrm{e}.\end{aligned} \tag{9}$$

In this "general" framework, the velocity is described by four functions of time, $h(t)$, $e(t)$, $f(t)$, $g(t)$, and by five vectors independent of time, $\hat{\mathbf{x}}_\mathrm{v}$, $\mathbf{p}$, $\hat{\mathbf{x}}_\mathrm{e}$, $\hat{\mathbf{y}}_\mathrm{e}$, $\hat{\mathbf{z}}_\mathrm{e}$. This is still too general to be applied to observations (which provide only one time series of $\mathbf{v}(t)$ per ICME). This equation shows that the trajectory of the center (described with $h(t)$, $\hat{\mathbf{x}}_\mathrm{v}$, $\mathbf{p}$) has a main effect on the observed velocity $\mathbf{v}(t)$, so on the observed characteristics of the ICME expansion (such as the difference between the front and back velocities).

### 2.2. Magnetic Structure

A subset of ICMEs, magnetic clouds (MCs), have a relatively well defined magnetic structure which can be modeled as a flux rope (see Section 1). Locally, at least along the part explored by the spacecraft, the flux rope can be considered as approximately straight since the size of the MC cross section ($\lesssim 0.1$ AU) is small in comparison to the radius of curvature of its axis ($\gtrsim 1$ AU).

**Hypothesis 5** We suppose a local invariance by translation of the magnetic configuration along the direction defined by $\hat{\mathbf{z}}_\mathrm{i}$. So, we can define locally a straight axis for the magnetic configuration.

This hypothesis permits to select the center at any location along the local MC axis. We select the center as the axial point closest from the spacecraft trajectory. This implies

$$\mathbf{p} \cdot \hat{\mathbf{z}}_\mathrm{i} = 0. \tag{10}$$

It is worth noting that Hypothesis 5 is compatible with the presence of a magnetic structure with the characteristics of a flux rope, but it does not require its presence. This is also the case for the following hypotheses (6 – 8). Then, the equations and the results of Sections 2.3 – 2.6 can be applied to more general magnetic configurations than a flux rope. In practice, the local invariant direction is obtained from MC data using the minimum variance method and/or a simultaneous fit to a flux rope model (see, *e.g.*, Lepping, Burlaga, and Jones, 1990; Dasso *et al.*, 2003; Gulisano *et al.*, 2007). Then, in what follows for concreteness we are more specific than theoretically needed when referring to the flux rope axis (rather than to the invariance direction).

### 2.3. Anisotropic Expansion

The expansion of ICMEs, and in particular of MCs, is expected to be not fully isotropic because of the anisotropy of their magnetic configuration and of their interaction with the solar wind. More precisely, a MC is formed by a magnetic flux rope, and thus the axial expansion is determined by a different physical evolution than the law determining the expansion in the plane perpendicular to its main axis. In the directions orthogonal to the axis, an anisotropy can also be present due to the interaction of the flux rope with the surroundings: *e.g.*, a compression could be present in the front if the flux rope is faster than the surrounding solar wind and/or in the back if the flux rope is overtaken by a faster stream.

**Hypothesis 6** From the physical origin of the expansion anisotropies, magnetic forces and interaction with the solar wind, we assume that the expansion direction $\hat{\mathbf{z}}_\mathrm{e}$ is along the flux rope axis, so $\hat{\mathbf{z}}_\mathrm{i} = \hat{\mathbf{z}}_\mathrm{e}$, and that the expansion direction $\hat{\mathbf{x}}_\mathrm{e}$ is defined by the interaction of the MC with the solar wind, so we set $\hat{\mathbf{x}}_\mathrm{e}$ in the plane $(\hat{\mathbf{x}}_\mathrm{v}, \hat{\mathbf{z}}_\mathrm{e})$, see Figure 1:

$$\hat{\mathbf{x}}_\mathrm{v} = \sin\gamma\,\hat{\mathbf{x}}_\mathrm{e} + \cos\gamma\,\hat{\mathbf{z}}_\mathrm{e}, \tag{11}$$

where $\gamma$ is the cone angle of the flux rope axis with respect to the global motion.

More precisely, we set $\hat{\mathbf{z}}_\mathrm{e}$ in the direction of the axial magnetic field such that $\mathbf{B}_\mathrm{axis} \cdot \hat{\mathbf{z}}_\mathrm{e} > 0$. Then, $\hat{\mathbf{y}}_\mathrm{e} = \hat{\mathbf{z}}_\mathrm{e} \times \hat{\mathbf{x}}_\mathrm{v} / |\hat{\mathbf{z}}_\mathrm{e} \times \hat{\mathbf{x}}_\mathrm{v}|$. This last definition is ambiguous when $\hat{\mathbf{z}}_\mathrm{e}$ is parallel to $\hat{\mathbf{x}}_\mathrm{v}$, so when the spacecraft crosses the flux tube along its axis, a case which is not present in observations. $\hat{\mathbf{x}}_\mathrm{e}$ completes the right handed orthonormal base $(\hat{\mathbf{x}}_\mathrm{e}, \hat{\mathbf{y}}_\mathrm{e}, \hat{\mathbf{z}}_\mathrm{e})$. Starting from $\hat{\mathbf{x}}_\mathrm{v}$, $\hat{\mathbf{z}}_\mathrm{e}$ is obtained by a rotation around $\hat{\mathbf{y}}_\mathrm{e}$ in an angle $\gamma$ [Equation (11)]. For $\gamma = \pm 90°$ the crossing is orthogonal to the flux rope, so the apex of the structure is crossed, while as $\gamma$ becomes closer to 0 or $\pm 180°$ the crossing is located more in one leg of the flux rope.

Equations (7), (10), and (11), with $\hat{\mathbf{z}}_\mathrm{i} = \hat{\mathbf{z}}_\mathrm{e}$, imply $\mathbf{p} \cdot \hat{\mathbf{x}}_\mathrm{e} = 0$, and so $\mathbf{p} = p\hat{\mathbf{y}}_\mathrm{e}$. Together with Equation (11), this implies that Equation (9) simplifies to

$$\mathbf{v}(t) = \sin\gamma \left[ h'(t) - h(t) \frac{e'(t)}{e(t)} \right] \hat{\mathbf{x}}_\mathrm{e}$$

$$+ p\frac{f'(t)}{f(t)}\hat{\mathbf{y}}_{\rm e} + \cos\gamma\left[h'(t) - h(t)\frac{g'(t)}{g(t)}\right]\hat{\mathbf{z}}_{\rm e}. \quad (12)$$

This corresponds to the velocity expressed in the flux rope, or MC frame, which was used previously to separate the azimuthal and axial magnetic field components (Dasso *et al.*, 2006). This frame is also adapted to study the expansion since it permits to separate the three principal directions of expansion.

It is also useful to have the velocity components in the frame $(\hat{\mathbf{x}}_{\rm v}, \hat{\mathbf{y}}_{\rm v}, \hat{\mathbf{z}}_{\rm v})$ which is closer to the observed (GSE) frame. $\hat{\mathbf{x}}_{\rm v}$ is defined by the velocity of the flux rope center ($\hat{\mathbf{x}}_{\rm v} = -\mathbf{v}_{\rm c}/v_{\rm c}$). We set $\hat{\mathbf{y}}_{\rm v}$ in the direction of minimum approach of the flux rope axis to simplify the expressions, so $\hat{\mathbf{y}}_{\rm v} = \hat{\mathbf{y}}_{\rm e}$.

Equation (12) rewrites in the $(\hat{\mathbf{x}}_{\rm v}, \hat{\mathbf{y}}_{\rm v}, \hat{\mathbf{z}}_{\rm v})$ frame as

$$\mathbf{v}(t) = \left[h'(t) - h(t)\left\{\sin^2\gamma\frac{e'(t)}{e(t)} + \cos^2\gamma\frac{g'(t)}{g(t)}\right\}\right]\hat{\mathbf{x}}_{\rm v} + p\frac{f'(t)}{f(t)}\hat{\mathbf{y}}_{\rm v} + h(t)\sin\gamma\cos\gamma\left\{\frac{e'(t)}{e(t)} - \frac{g'(t)}{g(t)}\right\}\hat{\mathbf{z}}_{\rm v}. \quad (13)$$

With $\hat{\mathbf{x}}_{\rm v} \approx \hat{\mathbf{x}}_{\rm GSE}$, $\hat{\mathbf{y}}_{\rm v}$ and $\hat{\mathbf{z}}_{\rm v}$ are deduced from a simple rotation around $\hat{\mathbf{x}}_{\rm GSE}$ of the vectors $\hat{\mathbf{y}}_{\rm GSE}$ and $\hat{\mathbf{z}}_{\rm GSE}$. Then, the expressions in GSE coordinates can be deduced easily from the expressions of $\mathbf{v}$ in the $(\hat{\mathbf{x}}_{\rm v}, \hat{\mathbf{y}}_{\rm v}, \hat{\mathbf{z}}_{\rm v})$ frame, when the direction of the closest approach, $\hat{\mathbf{p}}$, is known. This implies that the results obtained in the $(\hat{\mathbf{x}}_{\rm v}, \hat{\mathbf{y}}_{\rm v}, \hat{\mathbf{z}}_{\rm v})$ frame can be directly applied to observations.

Several general properties are shown by Equation (13):

- Along $\hat{\mathbf{x}}_{\rm v}$ we have a combination of the transverse and axial expansion rates with a weight defined by the square of the usual geometric projection factors. This implies that a crossing far from an orthogonal crossing (*i.e.*, far from $\hat{\mathbf{z}}_{\rm e} \perp \hat{\mathbf{x}}_{\rm v}$) is needed to have a significant contribution of the axial expansion in the observed $v_x$ component.
- Along $\hat{\mathbf{z}}_{\rm v}$ we have the difference of the expansion rates, this is an interesting property to determine the anisotropy of the expansion.
- Both $x$- and $z$-velocities components strongly depend on $h(t)$, so on the global motion of the MC center.
- Only the $y$-velocity component is a direct signature of the expansion rate; however, it is proportional to the impact parameter $p$, a quantity difficult to determine precisely in practice.
- For the same expansion along and across the axis, so $e(t) = g(t)$, the angle $\gamma$ is no longer present in Equation (13), as expected.

### 2.4. Global Motion

**Hypothesis 7** We describe the motion of the center by

$$h(t) = -\frac{a}{2}(t - t_{\rm c})^2 - V_{\rm c}(t - t_{\rm c}), \quad (14)$$

where $a$ is the constant acceleration and $V_c$ is the velocity of the center at $t = t_c$ (time of the closest approach of the spacecraft to the ICME center).

Notice that, since $\hat{\mathbf{x}}_v$ is oriented towards the Sun, $a < 0$ and $V_c > 0$ corresponds to the case of a fast ICME decelerating and moving outward from the Sun. This simplified description of the center dynamics is sufficient in most observed cases, since the acceleration of ICMEs is small enough that even the acceleration term in Equation (14) provides only a very small correction to the expansion derived from *in situ* velocity observations (see Section 3). Then, with Equation (14) included, Equation (13) becomes

$$\begin{aligned}\mathbf{v}(t) \approx & \left[-V_c - a(t-t_c)\right]\hat{\mathbf{x}}_v \\ & + \left[V_c(t-t_c) + \frac{a(t-t_c)^2}{2}\right]\left[\sin^2\gamma\,\frac{e'(t)}{e(t)} + \cos^2\gamma\,\frac{g'(t)}{g(t)}\right]\hat{\mathbf{x}}_v \\ & + \frac{pf'(t)}{f(t)}\hat{\mathbf{y}}_v \\ & - \left[V_c(t-t_c) + \frac{a(t-t_c)^2}{2}\right]\sin\gamma\cos\gamma\left[\frac{e'(t)}{e(t)} - \frac{g'(t)}{g(t)}\right]\hat{\mathbf{z}}_v. \end{aligned} \tag{15}$$

The two contributions of $a$ in the $x$-component have different magnitudes. Let us first define a typical expansion time $T$ by taking the minimum value of $e(t_c)/e'(t_c)$ and $g(t_c)/g'(t_c)$. This expansion time is typically comparable to the transit time of the ICME from the Sun to the spacecraft (usually more than two days, and frequently $\approx$ four days for a distance of 1 AU from the Sun); so, in general $T$ is much longer than half the crossing time (of the order or less than half a day). Then, the ratio of the second to the first contribution of $a$ in the $x$-component of Equation (15) is $\approx |t - t_c|/(2T) \ll 1$, since $|t - t_c|$ is bounded by half the crossing time. Then, we can neglect the second contribution of $a$ in the $x$ component. A term of similar magnitude is also present in the $z$ component of Equation (15), which then mainly depends on $V_c$ for the global motion contribution.

Next, we analyze the most important terms in Equation (15). Since in most ICMEs $|t - t_c|/(2T) \ll 1$ and $|a(t - t_c)| \ll V_c$ are well satisfied, we do a first order Taylor expansion of Equation (15):

$$\begin{aligned}\mathbf{v}(t) \approx & \left[-V_c - a(t-t_c) + V_c(t-t_c)\left\{\sin^2\gamma\,\frac{e'(t_c)}{e(t_c)} + \cos^2\gamma\,\frac{g'(t_c)}{g(t_c)}\right\}\right]\hat{\mathbf{x}}_v \\ & + \frac{pf'(t_c)}{f(t_c)}\left[1 + (t-t_c)\left\{\frac{f''(t_c)}{f'(t_c)} - \frac{f'(t_c)}{f(t_c)}\right\}\right]\hat{\mathbf{y}}_v \\ & - V_c(t-t_c)\sin\gamma\cos\gamma\left\{\frac{e'(t_c)}{e(t_c)} - \frac{g'(t_c)}{g(t_c)}\right\}\hat{\mathbf{z}}_v. \end{aligned} \tag{16}$$

Since $\hat{\mathbf{x}}_v$ $(= -\mathbf{v}_c/v_c)$ is mostly along $x_{GSE}$ in observations, Equation (16) shows that the often observed linear variation of $v_{x,GSE}(t)$ is a property of the global motion combined with the self-similar expansion, and not a consequence of a particular time variation of the expansion law. In other words, when the expansion time is long compared to the ICME crossing time and $V_c$ is nearly constant during the crossing, we will observe a linear profile for $v_x(t)$. Furthermore, for typical ICME expansion rates, the deceleration contribution still present in Equation (16) is also negligible (Section 3). We conclude that the observed almost linear profile of $v_{x,GSE}(t)$ in ICMEs can provide a measure of the expansion rate (more

precisely a combination of transverse and axial expansion rates), provided we take into account the global velocity $V_c$.

A similar linear dependence with time is present in the $z$ component with the same two origins: global and expansion motion (with a different contribution of the expansion than in the $x$ component). This contrasts with the expected nearly constant value of the $y$ velocity component, since the linear term in time in Equation (16) has two subtractive terms of similar magnitude. The presence of this $y$ component implies an observed bias of the global motion of the ICME: the observed velocity deviates from the real direction, $\hat{\mathbf{x}}_v$, by an amount proportional to the impact parameter and to the expansion rate in the $\hat{\mathbf{y}}_v (= \hat{\mathbf{y}}_e)$ direction. This implies that the often observed small deviation of the mean velocity in MCs from $x_{GSE}$ is not necessarily an evidence of a slightly non radial motion but could also be due to this aberration effect. This requires the determination of the spacecraft trajectory within the MC to estimate $\mathbf{p}$ and to rotate the data in the $(\hat{\mathbf{x}}_v, \hat{\mathbf{y}}_v, \hat{\mathbf{z}}_v)$ frame (in the $\hat{\mathbf{y}}_{GSE}$ and $\hat{\mathbf{z}}_{GSE}$, the $y_v$ and $z_v$ components of Equation (16) are usually mixed).

### 2.5. Expansion Law

The above Equations (15) and (16) are still too general for most applications to observations since they still contain three unknown functions, as well as free parameters. Here we introduce more physics to define the expansion rates. MHD models of expanding flux ropes usually find that the flux tube radius is expanding as a power law of distance $D$ to the Sun, with an exponent close to unity (*e.g.*, Chen (1996) found a dependence as $D^{0.88}$ between 0.3 and 5 AU). This is supported by the statistical results obtained on large samples of MCs and ICMEs, as follows. Bothmer and Schwenn (1994) found that the radial size of MCs behave as $D^{0.78\pm0.1}$ with $D$ between 0.3 and 4.2 AU. Leitner *et al.* (2007) found that the diameter of MCs behave as $D^{0.61\pm0.09}$ with $D$ between 0.3 and 7 AU, while the dependence is steeper, $D^{1.14\pm0.44}$, when the range of solar distances is limited below 1 AU. Moreover, Liu, Richardson, and Belcher (2005) and Wang *et al.* (2005) determined the size of a large set of ICMEs observed between 0.3 and 5.4 AU (a fraction being MCs). They found that the size of the ICMEs increases as $D^{0.92\pm0.07}$ and $D^{0.61}$, respectively.

**Hypothesis 8** With the above results, we suppose that the expansion factors are given by

$$e(t) = \left(\frac{D(t)}{D_o}\right)^l = \left[1 + \frac{t - t_c}{\tau} + \frac{\widetilde{a}}{2}\left(\frac{t - t_c}{\tau}\right)^2\right]^l, \tag{17}$$

and similar expressions for $f(t)$ and $g(t)$, simply replacing the exponent $l$ by $m$ and $n$, respectively. $D_o$ is the observing solar distance at the time of closest approach between the spacecraft and the ICME center ($D_o = D(t_c)$), $D(t) = D_o - h(t)$, $\tau = D_o/V_c$, and $\widetilde{a} = a\tau/V_c$. In practice both $|t - t_c|/\tau \ll 1$ and $\widetilde{a} \ll 1$ (see Sections 2.4 and 3), so the term with $\widetilde{a}$ in the previous equation is negligible. The spatial sizes of the flux rope at time $t_c$ (defined by the closest approach) are used as reference so that $e(t_c) = f(t_c) = g(t_c) = 1$. In any case, multiplying $e, f, g$ by a constant factor has no effect in the above equations (where only ratios, such as $e'/e$, are present).

With the observational results mentioned above, the exponents $l, m, n$ are expected to be in the range [0.6, 1], with plausible values outside this range for some special cases. Equation (17) is only supposed to be valid during the crossing time and a deviation from Equation (17) is expected close to the Sun. A test of the application range of Equation (17) will be possible with the heliospheric imagers of STEREO spacecrafts (Harrison *et al.*, 2008).

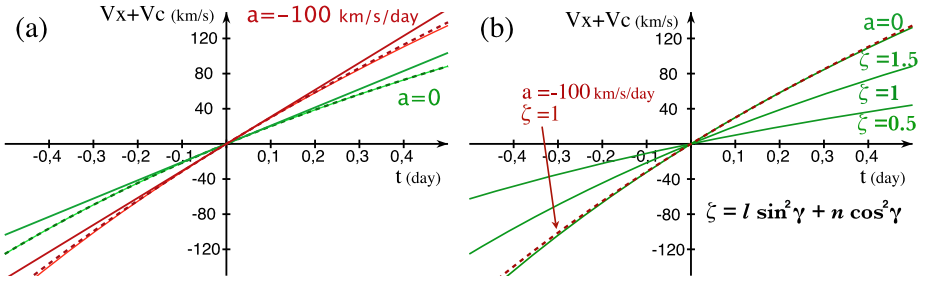


**Figure 2** Expected velocity component along the trajectory, relative to the center velocity, for an accelerated global motion [Equation (14)] and a self-similar expansion [Equation (17)]. The origin of time is set at the closest approach distance from the ICME center. The green and red lines are drawn without and with a large deceleration, respectively. The parameters are: $V_c = 600$ km s$^{-1}$, $\tau = 2.9$ day (transit time from the Sun to 1 AU with a constant velocity $V_c$). (a) Comparison of two deceleration values in the velocity profile for $\zeta = 1$. The nearby continuous and dashed lines take into account the deceleration fully [Equation (15)] and only in the global motion [Equation (18)], respectively. The straight continuous lines correspond to the first order Taylor expansion in $t - t_c$ [Equation (16)]. (b) Comparison of the effects of expansion and of a large deceleration. The case with a large deceleration and $\zeta = 1$ (dashed red line) is very close to the curve with no acceleration and $\zeta = 1.5$. For ICMEs, the effect of acceleration is expected to be much lower (see Section 3 and Table 1).

With Equation (17), neglecting the terms in $\widetilde{a}((t - t_c)/\tau)^2$, Equation (15) simplifies to

$$\begin{aligned}\mathbf{v}(t) \approx & \left[-V_c - a(t - t_c) + \frac{V_c(t - t_c)}{\tau + t - t_c}\left(l \sin^2\gamma + n\cos^2\gamma\right)\right]\hat{\mathbf{x}}_v \\ & + \frac{pm}{\tau + t - t_c}\hat{\mathbf{y}}_v \\ & + \frac{V_c(t - t_c)}{\tau + t - t_c}\sin\gamma\cos\gamma(n - l)\hat{\mathbf{z}}_v. \end{aligned} \tag{18}$$

Except for the global motion, $-V_c + a(t - t_c)$, all the velocity components are divided by $\tau + t - t_c$ which implies a moderate decrease with time, since, in practice for most ICMEs, the duration $\tau$ ($\approx$ transit time) is larger than two days, while half of the crossing time is lower than half a day.

## 2.6. Theoretical Velocity Profiles

We illustrate below the above equations using representative values of the parameters. From the observational results, summarized in Section 2.5, we have the mean values of the exponents $l, n$ in the range [0.6, 1]. Since the dependence on $l, n$ and $\gamma$ is simple, we only present figures where the parameter $\zeta = l\sin^2\gamma + n\cos^2\gamma$ is used. We also only draw $V_x + V_c$ since $V_z$ has a similar behavior with time, while $V_y$ is simpler (almost constant with time). We use a time interval of one day as a typical value for large ICMEs and MCs observed in the vicinity of Earth. Smaller events are simply represented by a portion of the central part of the plots.

The less known magnitude is the acceleration $a$ of the MC center. Can it compete with the expansion term in Equation (18)? The normalized acceleration, $\widetilde{a} = a\tau/V_c$, gives the relative contribution of the acceleration (with $\zeta \approx 1$). In Section 3, we find $|\widetilde{a}| \leq 0.2$ using three different methods, while the typical values in ICMEs observed at 1 AU, and beyond,

are expected to be much lower. Here, to illustrate the effect of the acceleration, we use a large value: $a = -100\ \mathrm{km\,s^{-1}\,d^{-1}}$ ($\approx -1.2\ \mathrm{m\,s^{-2}}$) giving $\widetilde{a} \approx -0.5$ for $V_c = 600\ \mathrm{km\,s^{-1}}$. The unit of the acceleration, $\mathrm{km\,s^{-1}\,d^{-1}}$ (d: days), is selected because it gives directly the modification of the velocity during the crossing time of the ICME. In the present case, the velocity of the center decreases by $100\ \mathrm{km\,s^{-1}}$ in one day, and the launch velocity for the CME center at the Sun is $\approx 900\ \mathrm{km\,s^{-1}}$, assuming a constant deceleration.

We compare the different velocity equations obtained in Sections 2.4 and 2.5 in Figure 2a. As shown in Section 2.4, the contribution of the acceleration is fully negligible in the expansion term. Indeed, even with $a$ as large as $-100\ \mathrm{km\,s^{-1}\,d^{-1}}$, there is nearly no difference between the dashed line [Equation (18)] and the nearby continuous line [Equation (15)], with the expansion functions defined by Equation (17).

Figure 2a also shows a visible, but still small difference between the two continuous lines representing the full terms [Equation (15)] and its Taylor expansion in time to the first order [Equation (16)]. Indeed, the change in the expansion rates, $e(t)$ and $g(t)$, during the crossing time can have a significant effect on the velocity profile only for a large crossing time $\Delta t$. Since $\Delta t/\tau \approx S/D$, where $S$ is the ICME spatial size, the deviation from a linear velocity profile with time is expected to be observable only in the largest ICMEs. Indeed, even in a huge event like the MC observed on the 29 October 2003, the curvature of the velocity profile is small (Mandrini *et al.*, 2007).

A deceleration as large as $-100\ \mathrm{km\,s^{-1}\,d^{-1}}$ can change significantly the slope of the observed profile (Figure 2). Since the effect of expansion and deceleration both give a dominant linear contribution to the velocity profile, they cannot be separated using only the observed velocity profile at one spacecraft. For example, a strong expansion $\zeta = 1.5$ with no acceleration, can be confused with a slower expansion $\zeta = 1$ and a deceleration of $-100\ \mathrm{km\,s^{-1}\,d^{-1}}$ (Figure 2b). However, as shown in Section 3, we expect this situation to be at most exceptional in observed ICMEs.

## 3. Acceleration of ICMEs/MCs

The aim of this section is to estimate the contribution of the acceleration in the observed in situ temporal profiles of the velocity. More precisely, we estimate the normalized acceleration, $\widetilde{a} = a\tau/V_c$ which gives the relative contribution of the acceleration to the expansion in Equation (18), using $\zeta = l\sin^2\gamma + n\cos^2\gamma \approx 1$ ($\zeta$ is estimated to be in the range [0.6, 1] in Section 2.5).

### 3.1. Information Provided by Type II Bursts

An interplanetary type II burst is interpreted as radio-frequency emission from the shock present in front of an ICME (Reiner *et al.*, 1998; Berdichevsky *et al.*, 2002). With an heliospheric density model, and assuming the type II emission to be radiated at the fundamental or second harmonic of the local plasma frequency (which varies as the square root of the plasma density), the radio frequency can be converted to a radial distance, so radio observations have the potentiality to monitor the velocity of the ICME shock from a few $R_\odot$ to close to the Earth and beyond. Since the solar-wind plasma density decreases almost as the inverse of the distance squared, the inverse of the radio frequency, $1/f$, varies as the distance. Then, in dynamic spectra plotted as $1/f$ function of time, a uniform velocity is traced out by drifting emission features located along straight lines (Reiner *et al.*, 1998; Hoang *et al.*, 2007).

From 42 cases, Reiner, Kaiser, and Bougeret (2007) deduced that the radio data are compatible with a constant deceleration close to the Sun, up to a distance $r_a$, and uniform velocity later on. The deceleration distance, $r_a$, is spread in the range (0.3, 1.5) AU. ICMEs which decelerate closer the Sun (lower $r_a$ value) have a stronger deceleration. From other cases, *e.g.*, Hoang *et al.* (2007), some ICMEs accelerate near the Sun; then, later on, they have an approximatively constant propagation speed in the interplanetary medium.

However, the above results from type II bursts provide only a small constraint on the acceleration of the ICME center, as follows. First, type II bursts have a broad band signature especially around 1 AU distance (see, *e.g.*, Figures 2 and 3 of Reiner, Kaiser, and Bougeret, 2007). This provides only a weak constraint on the local acceleration. But, more important, type II bursts are supposed to trace the shock in front of the ICME. Then, their velocity is the sum of the ICME center and expansion velocities, so indeed, it corresponds to all the terms in Equation (18). So, type II bursts cannot be directly used to estimate the acceleration of the ICME center.

Still, type II bursts indicate that the shocks dominantly decelerate closer to the Sun. This is an indication that the driver of the shock, the ICME behind, is also likely to decelerate dominantly closer to the Sun. Then, when a mean acceleration for the ICME center is determined between the Sun and in situ measurements, in the next three subsections, the derived mean acceleration is expected to be larger than the local acceleration when the ICME crosses the spacecraft.

### 3.2. Estimation of the Acceleration from Spacecrafts in Quadrature

An estimation of the acceleration can be done when the velocity is measured both in the corona and *in situ*. The most favorable case is when the coronagraph and the *in situ* observations are in quadrature since this configuration minimizes the projection effects for the coronal velocity (Burlaga *et al.*, 1982; Weiss *et al.*, 1996). The leading edge of the CME is usually associated with the front of the associated ICME. CMEs observed below the average slow solar wind velocity ($\approx 400\ \mathrm{km\,s^{-1}}$) are typically accelerated, while those above this velocity are decelerated (Lindsay *et al.*, 1999; Schwenn *et al.*, 2005). This result is classically interpreted as the result of the drag force between the ICME and the solar wind. The mean acceleration was derived by Gopalswamy *et al.* (2001) with observations between 0.6 and 0.9 AU (from PVO and Helios 1 spacecrafts) and by Rust *et al.* (2005) with observations between 1.2 and 1.8 AU (from NEAR and SOHO spacecrafts). However, similarly to type II bursts, this acceleration includes both the global motion and the expansion of the ICME.

In a fraction of limb CMEs, a bright core is observed at their center. Moreover, for MCs, the crossing of the central part of the flux rope can be estimated. Then, assuming that the bright core is located at the center of the flux rope, Rust *et al.* (2005) found an acceleration typically smaller by a factor $\approx 4$ for the center than for the leading edge. This implies that, in the eight studied MCs, the dynamics is mainly in the expansion of the magnetic structure (relative to its center). This result is in agreement with the analysis of two cases observed by Ulysses at a larger distance from the Sun ($\approx 4.6$ AU) since Funsten *et al.* (1999) found that the mean velocity of the center (computed from the transit time) was close to the in situ measured velocity while the leading edge was significantly faster.

Assuming a constant acceleration of the MCs, Rust *et al.* (2005) found an average acceleration of the CME center, from the Sun to the spacecraft, $a_c$, which depends on the coronal CME velocity, $u$. The least square fit to the data of a straight line gives: $a_c \approx 21(1 - u/340)\ \mathrm{km\,s^{-1}\,d^{-1}}$ (with $u$ in $\mathrm{km\,s^{-1}}$). With the same hypothesis, we obtain

the normalized acceleration:

$$\widetilde{a} = \frac{a_c \tau}{V_c} = \frac{2\widetilde{a}_u}{1 + 2\widetilde{a}_u + \sqrt{1 + 2\widetilde{a}_u}}, \tag{19}$$

where $\widetilde{a}_u = a_c D/u^2$ is the normalized acceleration using $u$. We use $D = 1.5$ AU as the mean distance of NEAR spacecraft from the Sun. $\widetilde{a}$ changes sign for $u = 340$ km s$^{-1}$, and takes its largest negative value for $u \approx 700$ km s$^{-1}$ with $\widetilde{a} \approx -0.13$. For larger $u$ values, $|\widetilde{a}|$ becomes sightly smaller (a factor 2 smaller is only obtained for $u \approx 2000$ km s$^{-1}$). Then, $|\widetilde{a}|$ is always small compared to $\zeta$ (which is expected to be in the range [0.6, 1], Section 2.5). Moreover, this result is an upper bound on the local deceleration magnitude since the deceleration is expected to be stronger closer to the Sun (Section 3.1). Then, the results of Rust *et al.* show that the deceleration of the MC center is expected to have a low contribution in the in situ observed velocity [*i.e.*, $\widetilde{a}$ is small compared to $\zeta$ in Equation (18)].

### 3.3. Estimation of the Acceleration Using a Large Number of ICMEs

Liu, Richardson, and Belcher (2005) did a statistical study of about 220 ICMEs observed in situ from 0.3 to 5.4 AU using data from Helios 1 and 2, WIND, ACE and Ulysses. They combined two criteria to localize ICMEs. The first one is an enhanced alpha-to-proton density ratio (greater than 0.08), and the second one is a low proton temperature (lower than half the value expected in the solar wind with the same speed). They cannot follow a given ICME with distance, but rather report on the ICME statistical properties with the distance $D$ to the Sun. They found that the bulk velocity can be fitted by

$$v(D) \approx v_1 (D/D_1)^{n_v}, \tag{20}$$

with $v_1 = 458 \pm 6$ km s$^{-1}$, $n_v = -0.002 \pm 0.02$, and $D_1 = 1$ AU. Wang *et al.* (2005) did a similar analysis on a larger set of possible ICMEs by only using the low temperature criteria. They found similar results: $v_1 = 456$ km s$^{-1}$ and $n_v = -0.003$.

The ICME acceleration is $a = \mathrm{d}v/\mathrm{d}t = v\,\mathrm{d}v/\mathrm{d}D$, so we derive the normalized acceleration $\widetilde{a}$:

$$\widetilde{a} \approx \frac{a}{v^2} = \frac{\mathrm{d}\log v}{\mathrm{d}\log D}. \tag{21}$$

Using Equation (20), $\widetilde{a} \approx n_v \ll 1$ from both studies.

However, the above estimation is mixing ICMEs with a probable broad range of accelerations (even acceleration with both signs). It is possible to estimate an order of magnitude for the maximum deceleration by considering only the fraction of the ICMEs having the largest velocities at all distances (if we make the reasonable hypothesis that a fast ICME will stay faster than average at all distances). Equation (20) gives an approximate tendency for the fastest ICMEs with $n_v \approx -0.15$ and $v_1 \approx 800$ km s$^{-1}$ when plotted on Figure 5 of Liu, Richardson, and Belcher (2005). Similarly, we consider the slowest ICMEs, then $n_v \approx 0.15$ and $v_1 \approx 300$ km s$^{-1}$ give an approximate global tendency. We conclude that $|\widetilde{a}| \leq 0.15$, so that the global acceleration is introducing a low contribution in the observed ICME profile of the velocity. However, it is worth to keep in mind that this is just an estimation of the mean acceleration using different ICMEs at different distances from the Sun, using a low number of ICMEs, then, it is not a strict upper bound on $|\widetilde{a}|$.

**Table 1** Acceleration from multi-spacecraft observations of four events. The rows present: the label of each event, the time of closest approach to the flux rope axis (in UT), the corresponding velocity (in $\mathrm{km\,s^{-1}}$), the time interval ($\Delta t$, in d) between observations of ACE and Ulysses, the relative radial distance between both spacecrafts ($\Delta r$, in AU), the relative helio-latitudes and helio-longitudes between ACE and Ulysses (in degrees), two estimations for the acceleration (in $\mathrm{km\,s^{-1}\,d^{-1}}$), and the normalized acceleration ($\langle\widetilde{a}\rangle = \langle a\rangle\langle D\rangle/\langle V\rangle^2$).

| Event | Feb'99 | Aug'99 | Mar'00 | Jan'05 |
|---|---|---|---|---|
| Axis time (ACE) | 01:30, Feb. 19 | 01:00, Aug. 3 | 08:00, Mar. 19 | 10:30, Jan. 22 |
| Axis time (Ulysses) | 21:00, Mar. 04 | 18:00, Aug. 19 | 22:00, Mar. 31 | 12:00, Feb. 02 |
| $V_{\mathrm{axis}}$ (ACE) | $580 \pm 5$ | $375 \pm 15$ | $380 \pm 15$ | $780 \pm 15$ |
| $V_{\mathrm{axis}}$ (Ulysses) | $440 \pm 5$ | $400 \pm 15$ | $400 \pm 15$ | $680 \pm 15$ |
| $\Delta t$ | $13.8 \pm 0.3$ | $16.7 \pm 0.1$ | $12.6 \pm 0.1$ | $10.8 \pm 0.3$ |
| $\Delta r$ | 4.0 | 3.7 | 2.7 | 4.3 |
| Relative lat. | 22 | 38 | 43 | 17 |
| Relative long. | 1 | 147 | 9 | 27 |
| $\langle a\rangle$ | $-10.1 \pm 0.5$ | $1.5 \pm 1.3$ | $1.6 \pm 1.7$ | $-9.3 \pm 2$ |
| $a_1$ | $-11.1 \pm 1.6$ | $1.1 \pm 1.8$ | $-1.3 \pm 2.4$ | $-16 \pm 4$ |
| $\langle\widetilde{a}\rangle$ | $-0.20 \pm 0.01$ | $0.05 \pm 0.04$ | $0.04 \pm 0.05$ | $-0.09 \pm 0.02$ |

### 3.4. Estimation of the Acceleration from Multi-spacecraft Observations

Previous studies have analyzed the evolution of a given ICME/MC at different radial distances from the Sun, using observations made by more than one spacecraft (Cane, Richardson, and Wibberenz, 1997; Mulligan and Russell, 2001; Riley *et al.*, 2003; Foullon *et al.*, 2007; Rodriguez *et al.*, 2008).

From *in situ* velocity measurements, the observing time difference and the distance between the two spacecrafts, several estimations of the acceleration are available. As a first order approximation, we estimate the time, $t_i$, of the closest approach to the cloud axis as the center of the time interval when the MC is crossing spacecraft "$i$" (see Section 5 for an improved method). The difference of the anti-sunward velocity at the two spacecrafts, $\Delta V = V_2 - V_1$, over the time difference, $\Delta t = t_2 - t_1$, provides the mean acceleration, $\langle a\rangle$, during the travel time between the spacecrafts:

$$\langle a\rangle = \Delta V/\Delta t. \tag{22}$$

Since the distance, $\Delta r$, between the spacecrafts is known, assuming a constant acceleration, two other estimates of the acceleration are

$$a_1 = 2\big(\langle v\rangle - V_1\big)/\Delta t, \tag{23}$$

$$a_2 = 2\big(V_2 - \langle v\rangle\big)/\Delta t, \tag{24}$$

with $\langle v\rangle = \Delta r/\Delta t$. However, the three estimates are related by $\langle a\rangle = (a_1 + a_2)/2$.

The above estimations of the acceleration are applied to the four events previously studied by Riley *et al.* (2003), Liu *et al.* (2006), and Foullon *et al.* (2007). For example, the first MC in Table 1 was observed by ACE (at the Lagrangian L1 point) and by Ulysses (at 5 AU from the Sun). In this event the spacecrafts are located at approximately the same helio-longitude, but they are separated by an helio-latitude of 22°. When observed at ACE, the bulk

velocity of the flux rope center was $\approx 580$ km s$^{-1}$, while at Ulysses it was $\approx 440$ km s$^{-1}$, an observation consistent with the expected deceleration because the ejecta was traveling faster than the surrounding solar wind ($V_{sw} \approx 400-450$ km s$^{-1}$ in the front of the flux rope, when observed by ACE). We obtain similar values of the acceleration: $\langle a \rangle \approx -10$ and $a_1 \approx -11$ (in km s$^{-1}$ d$^{-1}$) which are coherent within the computed uncertainties.

Two of the events presented in Table 1 (Feb'99 and Jan'05) travel faster in the interplanetary medium ($V \approx 600$–$800$ km s$^{-1}$) while the other two travel slower (Aug'99 and Mar'00, $V \approx 400$ km s$^{-1}$, so at a speed typical of the solar wind). The two faster events have a small deceleration ($\approx -10$ km s$^{-1}$ d$^{-1}$). For the two slower MCs, our estimations for the accelerations are lower by an order of magnitude. Indeed the magnitude of the error bars does not permit a reliable estimate of their acceleration. Moreover, these two slow events are observed with a larger angular separation between the two spacecrafts, which adds the bias introduced by the unknown global shape of the MC structure. This implies an even more uncertain estimation of $a_1$ (mainly from $\Delta t$ which is present twice in $a_1$), and to a less extent of $\langle a \rangle$ (since the radial velocity, $V$, is expected to be relatively homogeneous across the MC at a given distance of the Sun). We can just conclude that $|a|$ is below few km s$^{-1}$ d$^{-1}$ for the two slower events.

As in the previous section, we estimate the normalized acceleration $\widetilde{a} = a\tau/V_c \approx a D/V_c^2$. Since $\langle a \rangle$ has the lowest uncertainty, we just show $\langle \widetilde{a} \rangle \approx \langle a \rangle \langle D \rangle / \langle V \rangle^2$ in Table 1. $\langle D \rangle$ is estimated as the mean radial distance between the spacecrafts ($= 1 + \Delta r/2$), and $\langle V \rangle = (V_1 + V_2)/2$. We find that $|\langle \widetilde{a} \rangle|$ is within the expected values of previous sections (the largest value of $|\langle \widetilde{a} \rangle|$ for Feb'99 is only slightly larger). We note that these values could be magnified compared to the values obtained at 1 AU because $\langle \widetilde{a} \rangle$ is proportional to $\langle D \rangle$ and we use $\langle D \rangle$ ($\approx 3$ AU). At the opposite, acceleration values are expected to be smaller at large distances. Which effect dominates is presently not known.

Taking into account the uncertainties and the possible different biases in the approaches, the results from observations in quadrature, for a large number of ICMEs and from two spacecrafts are in remarkable agreement. This implies that the ICME global acceleration (acceleration of its center) has only a small effect in the *in situ* observed velocities. This justifies a posteriori the hypothesis of a constant velocity frequently used in previous papers (*e.g.*, a number of those cited in Section 1); while this conclusion contrasts with other papers where deceleration is supposed to be the main origin of the observed decreasing velocity with time (see, *e.g.*, Hu *et al.* (2005) and references therein).

## 4. Distortion of the Observed Magnetic Field

The expansion, combined with the global motion, affects the time evolution of the measured magnetic field. The expected distortion of the observed magnetic field due to expansion has been analyzed by previous authors for particular cases (*e.g.*, Farrugia, Osherovich, and Burlaga, 1995). We analyze below these effects and give theoretical expressions for a general (anisotropic) self-similar expansion and non-null impact parameter, and then apply them to a particular initial field configuration and an isotropic expansion, extending previous studies.

### 4.1. General Equations

Combining the rectilinear motion of the ICME center [Equation (8)] with the observation at a given spatial position $\mathbf{r}(t) = \mathbf{r}_{sc}$, Equation (3) gives the observed position in the local

coordinates:

$$\begin{aligned} x_{\mathrm{e}}(t) &= -h(t)\sin\gamma, \\ y_{\mathrm{e}}(t) &= +p, \\ z_{\mathrm{e}}(t) &= -h(t)\cos\gamma. \end{aligned} \tag{25}$$

Then, any evolution model of an ICME magnetic field, defined in the local frame as $\mathbf{B}_{\mathrm{model}}(x_{\mathrm{e}}, y_{\mathrm{e}}, z_{\mathrm{e}}, t)$, can be transformed with Equation (25) to a function of time only. The simulation of the observed field is

$$\mathbf{B}_{\mathrm{observed}}(t) = \mathbf{B}_{\mathrm{model}}\big(-h(t)\sin\gamma,\, p,\, -h(t)\cos\gamma,\, t\big). \tag{26}$$

More specifically, let us consider the self-similar expansion of the field $\mathbf{B}(x_{\mathrm{e}}(t_0), y_{\mathrm{e}}(t_0), z_{\mathrm{e}}(t_0))$ defined at the time $t_0$. The self-similar expansion means a rescaling of the spatial coordinates according to Equation (4). The conservation of magnetic flux implies a modification of the field strength. Then, we obtain

$$\begin{aligned} B_x(t) &= B_x(x_{\mathrm{e}}/e, y_{\mathrm{e}}/f, z_{\mathrm{e}}/g)/(fg), \\ B_y(t) &= B_y(x_{\mathrm{e}}/e, y_{\mathrm{e}}/f, z_{\mathrm{e}}/g)/(eg), \\ B_z(t) &= B_z(x_{\mathrm{e}}/e, y_{\mathrm{e}}/f, z_{\mathrm{e}}/g)/(ef), \end{aligned} \tag{27}$$

where $x_{\mathrm{e}}, y_{\mathrm{e}}, z_{\mathrm{e}}, e, f, g$ are taken at time $t$ (given by Equations (25) and (17), respectively). This implies in general the transformation of the electric current (from Ampere's law) and the modification of the Lorentz force. Then, an initial force-free field will stay force-free only if $e = f = g$ (or the expansion is no longer self-similar). In MCs, the plasma $\beta$ is typically in the range $[10^{-2}, 10^{-1}]$ and the field is almost force-free; then, if the expansion is close to a self-similar expansion, it is expected to be almost isotropic.

### 4.2. Example of a Magnetic Configuration

In order to illustrate the effects of the expansion on the observed magnetic field, we consider an explicit example based on the Lundquist's solution:

$$\begin{aligned} \mathbf{B}(t) = &-\frac{p}{r}\frac{B_{\mathrm{o}}}{e^2(t)} J_1\big(\alpha_{\mathrm{o}} r/e(t)\big)\hat{\mathbf{x}}_{\mathrm{e}}, \\ &-\frac{h(t)\sin\gamma}{r}\frac{B_{\mathrm{o}}}{e^2(t)} J_1\big(\alpha_{\mathrm{o}} r/e(t)\big)\hat{\mathbf{y}}_{\mathrm{e}}, \\ &+\frac{B_{\mathrm{o}}}{e^2(t)} J_0\big(\alpha_{\mathrm{o}} r/e(t)\big)\hat{\mathbf{z}}_{\mathrm{e}}, \end{aligned} \tag{28}$$

with $r = \sqrt{h(t)^2\sin^2\gamma + p^2}$ and $B_{\mathrm{o}}$ is the central magnetic field strength. We set $e(t) = f(t) = g(t)$ so that the field stays force-free. This equation is a generalization of the ones derived by Shimazu and Vandas (2002) and Berdichevsky, Lepping, and Farrugia (2003) for the particular case of a linear time dependence of the expansion rate $e(t)$ (and isotropic expansion, so $l = m = n = 1$). Any particular anisotropic expansion (*i.e.*, given rates $e(t)$, $f(t)$, $g(t)$), as for example the case with only radial expansion ($l = m = 1, n = 0$,

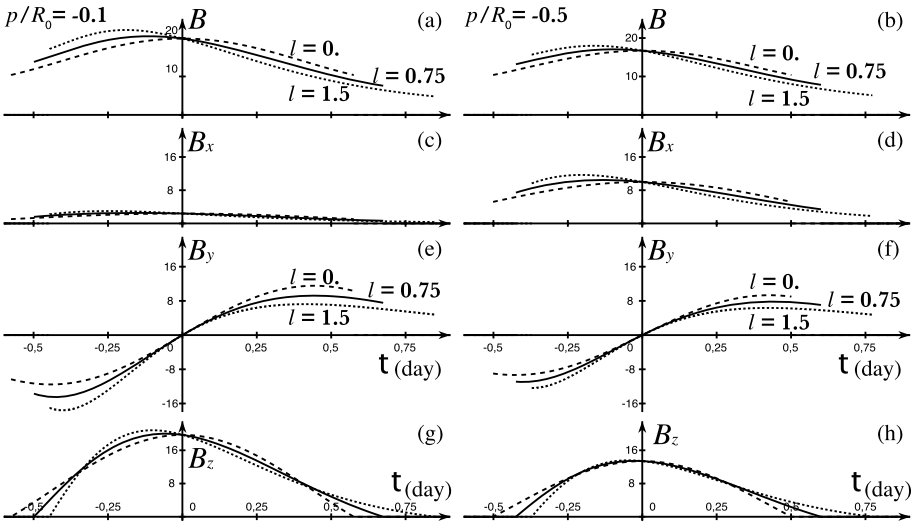


**Figure 3** Magnetic field components simulated along the spacecraft trajectory for an isotropic expansion ($l = m = n$). The field is plotted in the interval where $B_z > 0$. The expansion factor is set to 0, 0.75, and 1.5 to illustrate the cases without, with typical, and with strong expansion, respectively. Two values of the impact parameter $p$ (relative to the MC radius) are shown in the left/right panels. The origin of time is set at the closest approach distance from the flux rope center ($t_c = 0$). The parameters are: $V_c = 600$ km s$^{-1}$, $\tau = 2.9$ d (equal to the transit time from the Sun to 1 AU with a velocity $V_c$), $R_0 = 0.2$ AU, $a = 0$, $B_0 = 20$ nT.

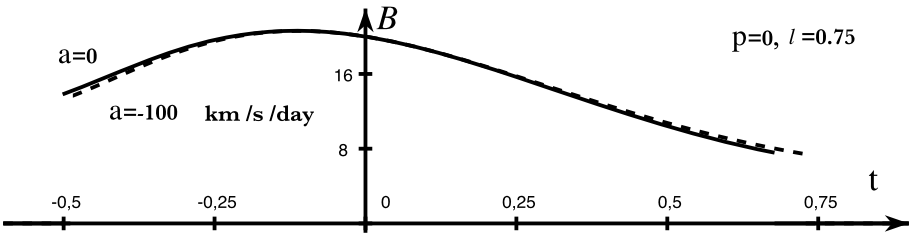


**Figure 4** Even a strong deceleration of the global motion has a low effect on the magnetic profile. The parameters are the same as in Figure 3, except for $p = 0$, and we consider a typical expansion factor of 0.75 (giving a moderate asymmetry of the magnetic profile).

*e.g.*, Farrugia, Osherovich, and Burlaga, 1995), can also easily be generalized by using Equation (27). Moreover, we explicitly write in Equation (28) the expected field along the spacecraft trajectory taking into account the parameters of the crossing (angle $\gamma$ and impact parameter $p$) as well as a general motion of the ICME center ($h(t)$), supposing only a rectilinear motion.

For concreteness, we consider the field of Equation (28) in the range where $B_z > 0$, so $J_0(\alpha_0 R_0) = 0$ where $R_0$ is the radius of the flux rope. Figure 3 shows the effects of the expansion and of the impact parameter; they are generalizations of previous studies where only a radial expansion was considered (*e.g.*, Figure 5 in Farrugia, Osherovich, and Burlaga (1995)). For all the curves, the magnetic configuration is the same at the time of closest approach ($t = t_c = 0$). Without expansion ($l = 0$) the field components are symmetric ($B_x$, $B_z$) or antisymmetric ($B_y$) with respect to the closest approach time.

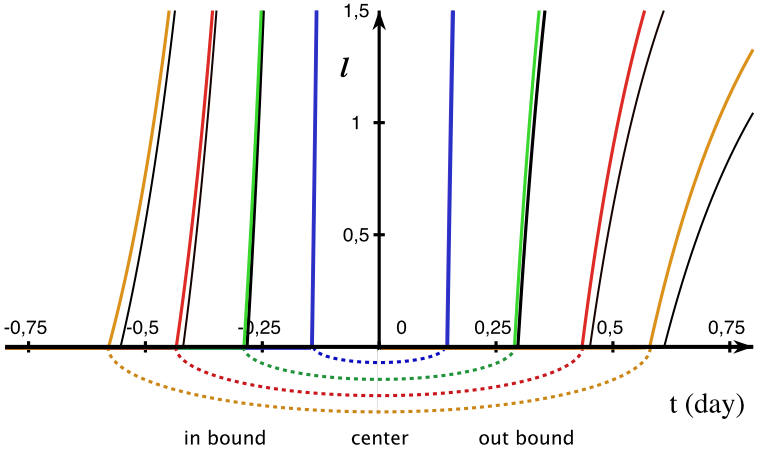


**Figure 5** Expected asymmetry between the in- and out-bound due to the expansion (aging effect). There is no expansion on the abscissa axis ($l = 0$), while the expansion is strong at the top of the plot ($l = 1.5$). For a given $l$, the curves with the same color represent the same flux surface located in the in- and out-bound at the same distance from the center for a given time $t$. However, the out-bound is observed later than the in-bound so when the flux rope is larger giving the observed asymmetry. The flux rope center is always set at $t = 0$ on the ordinate axis. At $t = 0$, the distance from the center of the blue, green, red and yellow positions in the in- and out-bound are 0.05, 0.1, 0.15 and 0.2 AU, respectively. These positions are computed with $a = 0$, while the nearby thin black lines are for $a = -100$ km s$^{-1}$ d$^{-1}$. The parameters are: $V_c = 600$ km s$^{-1}$, $\tau = 2.9$ d, $p = 0$, and $\gamma = 90°$.

An asymmetry in the observed field is present when the flux rope expands, as follows. For large $l$ values the size of the magnetic structure is smaller in the in-bound branch and larger in the out-bound one; both effects are stronger with a larger absolute time difference with the closest approach time (so with a larger $|t|$ in Figure 3, as $t_c = 0$). Then, for large $l$ values, the in-bound is observed during a shorter time interval (this being stronger in the front), and the out-bound is observed during a longer time interval (this being more significant in the back). Moreover, the magnetic flux conservation implies a stronger field in front and a weaker one in the back. Both effects are called "aging", and are partially responsible of the asymmetry observed in MC fields (besides a possible intrinsic asymmetry that could be present in the magnetic configuration). The aging asymmetry is most detectable on the absolute value of **B**, $B$, and it affects dominantly $B_y$ because the asymmetry is larger away from the closest distance position (where $B_y$ dominates). The aging distortion is also well present for a large impact parameter (Figure 3b). Then, it also affects $B_x$ significantly.

The effect of the global deceleration is small even for large values of "$a$"; this effect, shown in Figure 4, would be masked by magnetic fluctuations in any observed field. The deceleration has a low effect because it appears only in $h(t)$ in Equation (28); so, it has the same low effect than the second contribution of "$a$" in Equation (15), as shown in Section 2.4.

### 4.3. Asymmetry Between In-bound and Out-bound: Aging Effect

The aging effect, illustrated in Figure 3 for a particular field, can be analyzed in a more general way independently from the magnetic profile. Let us consider a flux rope with an azimuthal symmetry. The flux surface defined by a given radius, $\rho$, at time $t_c$ is located at

$\rho e(t)$ at time $t$. Then, the flux surface is observed at the two times, $t_-$ (in-bound) and $t_+$ (out-bound), satisfying the Pythagorean relationship:

$$h^2(t_\pm)\sin^2\gamma + p^2 = \rho^2 e^2(t_\pm). \tag{29}$$

Following the conclusions of Section 2.4 (see also Figure 5), one can neglect the deceleration in the expression of $h(t)$ given by Equation (14) and expand the equation in $(t - t_c)/\tau$ with $e(t)$ given by Equation (17). To the first order in $(t - t_c)/\tau$ we get

$$t_\pm \approx t_c + \frac{l\rho^2}{\tau(V_c \sin\gamma)^2} \pm \frac{\rho}{V_c \sin\gamma}\sqrt{\left(\frac{l\rho}{\tau V_c \sin\gamma}\right)^2 + 1 - \left(\frac{p}{\rho}\right)^2}, \tag{30}$$

where we have neglected terms in $\tau^{-2}$ compared to the terms in $(V_c/\rho)^2$ since the ratio of these terms is $\approx (\rho/D)^2 \ll 1$. However, we have kept the term in $(l/\tau)^2$ in the square root so that the closest approach (for $\rho = p$) is at time $t_c$. The asymmetry introduced by the expansion is associated to the term in $(l/\tau)(\rho/V_c \sin\gamma)^2$, it shifts both $t_-$ and $t_+$ later; so as this term increases, $t_-$ becomes closer to $t_c$ and $t_+$ becomes farther from $t_c$. The asymmetry increases quadratically with the distance to the axis (see Figure 5).

There is also a secondary effect of the expansion linked to the presence of $l$ inside the square root. This term increases slightly the crossing time, $t_+ - t_-$, as $l$ increases. However, when $\rho$ is significantly above its minimum value $p$, so far from the closest approach, this term has a magnitude of the order of $\rho^2/(\tau V_c)^2 \approx (\rho/D)^2 \leq 10^{-2}$, compared to $1 - (p/\rho)^2$. Then, one can simplify Equation (30):

$$t_\pm \approx t_c + \frac{\rho}{V_c \sin\gamma}\left[\frac{l\rho}{\tau V_c \sin\gamma} \pm \sqrt{1 - \left(\frac{p}{\rho}\right)^2}\right]. \tag{31}$$

We conclude that the time interval, $t_+ - t_-$, between the two crossings of the same flux surface is weakly affected by the expansion, as follows. With $p \ll \rho$, so far from the closest approach, the ratio of the asymmetry in time to the time interval $t_+ - t_-$ is $\approx l\rho/(\tau V_c \sin\gamma)$ $\approx l\rho/(D \sin\gamma)$, with $D$ being the distance of observation from the Sun. With the observed expansion $l$ of the order of unity (see Section 5, $l \approx 0.8 \pm 0.2$), this normalized asymmetry is typically of the order $\rho$ expressed in units of distance to the Sun. It implies that the asymmetry remains small for most MCs and it is only the largest MCs (Figure 5) and/or those crossed in one leg ($\sin\gamma$ small) which are expected to show a strong asymmetry due to the aging effect.

## 5. Examples of Velocity Observations

The aim of this section is to provide a simple application of the equations derived in Section 2 to *in situ* data, while a more extended application will be done in a later paper. We show first a detailed and precise analysis made for two MCs, and then we extend the analysis and present results for a set of MCs.

### 5.1. Two Magnetic Cloud Examples

The first MC (April, 2001) is slow, while the second one (November, 2004) is very fast. For more details on these two MCs see Nakwacki *et al.* (2008) and Dasso *et al.* (2007),

**Table 2** Main characteristics of the two MCs shown in Figures 6 and 7. From top to bottom: start and end times (day-month-year hh:mm) of the cloud as observed by Wind, orientation of the cloud axis from normalized minimum variance (azimuth, $\theta$, longitude, $\phi$, and angle between the MC axis and the $x_{\rm GSE}$ direction, $\gamma$), translation velocity ($-\langle V_{x,\rm GSE}\rangle$), mean radius, transit time ($=1$ AU$/\langle -V_{x,\rm GSE}\rangle$), $\zeta$ computed from the fitted slope of Equation (32) to the observed $V_{x,\rm GSE}(t)$.

| | April 2001 | November 2004 |
|---|---|---|
| Start | 22-Apr-2001 00:54 | 09-Nov-2004 20:30 |
| End | 23-Apr-2001 01:24 | 10-Nov-2004 10:20 |
| $\theta$ | $-62°$ | $-24°$ |
| $\phi$ | 274° | 275° |
| $\gamma$ | 88° | 85° |
| $-\langle V_{x,\rm GSE}\rangle$ | 360 km s$^{-1}$ | 785 km s$^{-1}$ |
| Mean radius | 0.11 AU | 0.12 AU |
| Transit time | 4.8 d | 2.2 d |
| $\zeta$ | 0.77 | 0.70 |

respectively. The two MCs are formed by a flux rope with a typical mean radius observed at 1 AU ($\approx$0.1 AU). However, the event of April 2001 is weaker ($B \approx 15$ nT) and slower ($\langle V_{x,\rm GSE}\rangle = -360$ km s$^{-1}$) than the event of November 2004 ($B \approx 40$ nT, $\langle V_{x,\rm GSE}\rangle = -785$ km s$^{-1}$). For an analysis of the solar wind conditions and solar sources for the MC of November 2004 see Harra *et al.* (2007) and Longcope *et al.* (2007).

*In situ* observations of plasma and magnetic properties of the MCs are measured by the instruments Solar Wind Experiment (SWE) and Magnetic Field Instrument (MFI), using a time cadence of 100 sec for SWE and 3 sec for MFI; both instruments are aboard the Wind spacecraft. We analyze observations of $V_{x,\rm GSE}$ (which is basically the component of the velocity in the direction of $\hat{\mathbf{x}}_{\rm v}$) and, thus, we expect to observe the profile described in Equation (18).

When $\widetilde{a} \ll 1$ (Section 3) and $|t - t_{\rm c}|/(2\tau) \ll 1$, a first order Taylor expansion of the $x$-component of Equation (18) gives

$$V_{x,\rm v}(t) \approx -V_{\rm c} + \frac{V_{\rm c}\zeta}{\tau}(t - t_{\rm c}), \tag{32}$$

$$\zeta = l \sin^2\gamma + n\cos^2\gamma. \tag{33}$$

We estimate $V_{\rm c}$ with $\langle V_{x,\rm GSE}\rangle$ inside the MC boundaries, and similarly $\tau = D/\langle -V_{x,\rm GSE}\rangle$ with $D = 1$ AU. Thus, we obtain an estimation of the expansion parameter $\zeta$ from the slope of a linear fitting of Equation (32) to the observed $V_{x,\rm GSE}$ time series. For both MCs, beyond some fluctuations (*e.g.*, waves), a clear linear trend is present in $V_{x,\rm GSE}$ (Figures 6 and 7).

We apply the minimum variance method to the normalized magnetic field vector ($\mathbf{B}/B$) to obtain the orientation of the MC axis as defined by $\theta$ (angle between the ecliptic plane and the cloud axis) and $\phi$ (angle between the projection of the axis on the ecliptic plane and $\hat{x}_{\rm GSE}$). We use the normalized magnetic field to minimize the bias introduced by the decay of $B$ due to the aging of the cloud (Gulisano *et al.*, 2007). The two MCs present values of $\gamma$ close to 90° (Table 2). Thus, for the two MCs, $\zeta \approx l$ (*i.e.*, the observed expansion along $\hat{x}_{\rm GSE}$ corresponds mainly to the $\hat{\mathbf{x}}_{\rm e}$ direction).

We obtain a very similar expansion parameter $\zeta$ (0.77 and 0.7) for the two MCs, so we conclude that they are expanding with a similar law! This result was not obvious from the

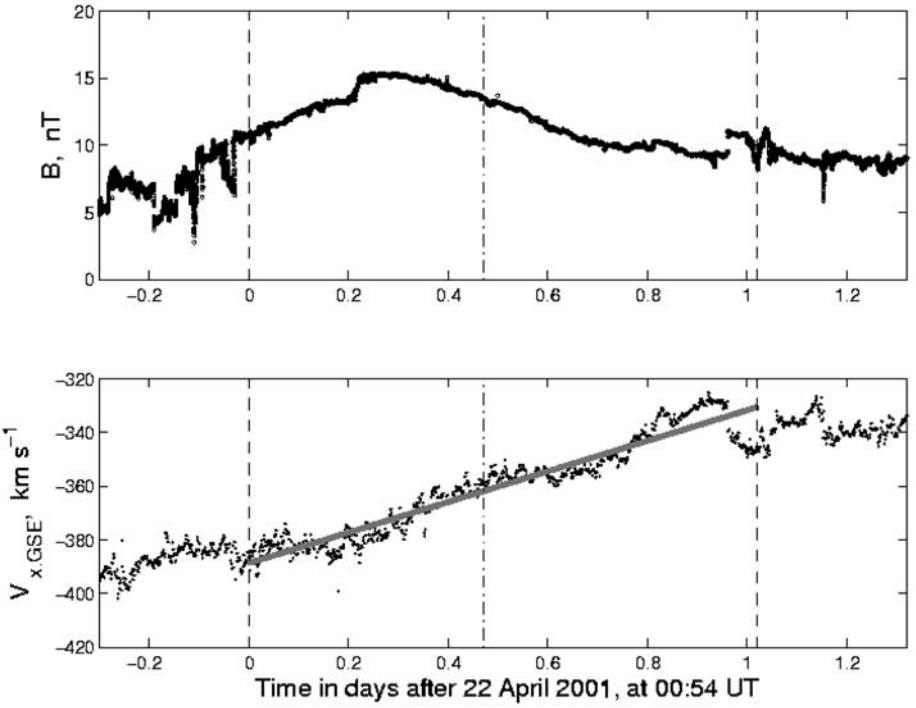


**Figure 6** Example of a slow and typical MC in expansion. Upper panel: magnetic field strength. Lower panel: velocity component $V_{x,\mathrm{GSE}}$ and fitted curve (gray line). In both panels the dashed vertical lines indicate the start and end of the cloud, and the dash-dotted vertical line shows the time at which Wind was at the closest approach to the MC axis (22 April 2001, 06:49 UT).

data since the difference in velocity between the front and back part of the MCs, $V_{\mathrm{front}} - V_{\mathrm{back}}$, is larger by more than a factor 2 for the second MC compare to the first one ($\approx 150$ compared to $\approx 60$ km s$^{-1}$). Indeed, the second MC is crossed in a shorter time (factor $\approx 0.6$), so that the variation per unit time of the measured velocity is a factor 4 larger in the second MC than in the first one. However, these differences, directly deduced from the data, are just apparent. Equation (32) shows that this is simply due to the larger mean velocity of the second MC (and not an effect of a stronger expansion).

For both MCs, $B$ has an expected asymmetry with stronger fields in the front (Figure 3). However, in both cases the maximum of the magnetic field is observed at earlier times than the expected time from the aging effect applied to a symmetric structure (as marked by the dashed-dotted line in Figures 6 and 7). Indeed, the asymmetry introduced with $l = 0.75$ in Figure 3 is much less important than the one present in both MCs (Figures 6 and 7). Therefore, these data indicate the existence of an intrinsic spatial asymmetry in these MCs.

### 5.2. Results for a Set of Magnetic Clouds

We study the expansion of MCs already identified in previous studies (Table 3). Most of the MCs have been observed by Wind as the ones above, but a few have been observed by the Advanced Composition Explorer (ACE), the magnetic field observations come from the *Magnetic Field Experiment* (MAG) and the plasma data from the *Solar Wind Electron Proton Alpha Monitor* (SWEPAM).

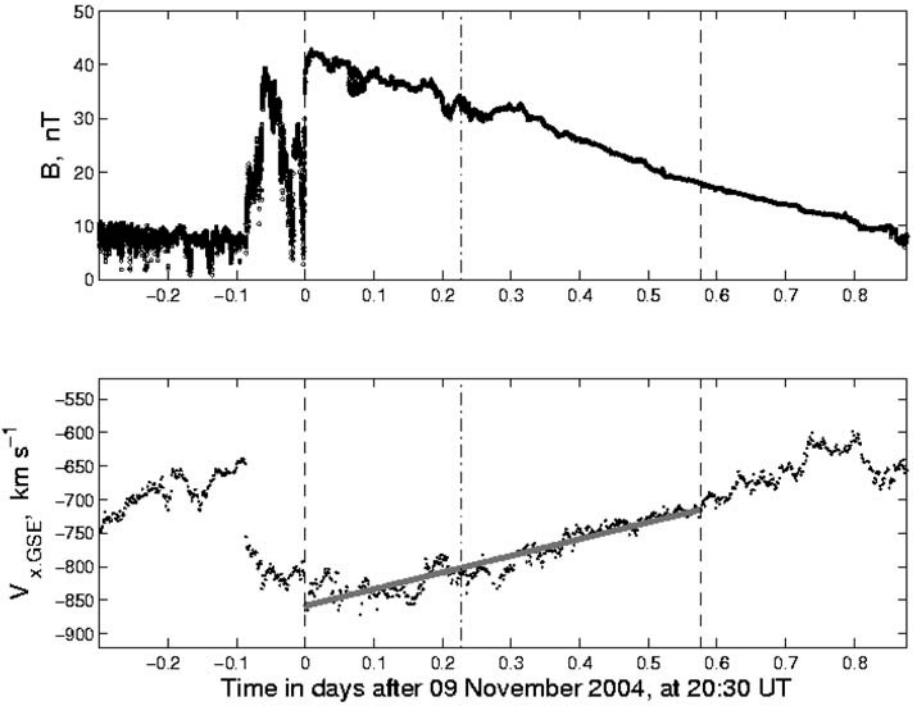


**Figure 7** Example of a large and fast MC. The same quantities as in Figure 6 are plotted for the MC observed by Wind on 9 November 2004. Wind was at the closest approach to the MC axis on 10 November 2004, 02:02 UT.

About half of the MCs we analyze have a well defined linear profile for $V_{x,\mathrm{GSE}}(t)$, comparable to those shown in Figures 6 and 7. For the other half, $V_{x,\mathrm{GSE}}(t)$ is nearly linear only in a fraction of the MC. While this fraction is typically larger than half the MC extension, this subset of MCs usually has an overtaking faster flow in their back. The overtaking flow could be associated to another MC, or an ICME or simply a fast solar wind stream. Then, we keep here only the MCs which are not overtaken (Table 3).

We keep the same MC boundaries as defined in the previous studies. The precise location of the MC boundary is not crucial to define $\zeta$ since it is the normalized slope of $V_{x,\mathrm{GSE}}(t)$ [Equation (32)]. The observed velocities depart from a linear temporal trend mostly near the boundaries of the MCs, this is a natural consequence of the interaction of each MC with its surrounding solar wind. In order to avoid these local perturbations, we define the velocity difference between the front and back boundaries, $\Delta V_x$, from the linear fit of Equation (32) to the data. Since we select not overtaken MCs, $\Delta V_x$ is close to the observed velocity difference, but it still represents better the global expansion of the MC.

The analyzed MCs have durations and field strengths spanning one order of magnitude while their mean values are typical of MCs observed at 1 AU (approximately 1 d and 20 nT, Table 3). $V_\mathrm{c}$ changes at most by a factor 3, and indeed this is about the maximum range of observed velocities in MCs ranging from slightly slower than the slow solar wind to exceptionally fast events with $V_\mathrm{c} \approx 1000$ km s$^{-1}$. The difference of velocity between the MC front and back has the largest variation, a factor $\approx 30$, with again a typical mean $\approx 130$ km s$^{-1}$. We conclude that the MCs selected are typical ones, with all main parameters having values covering the typical ranges for MCs observed at 1 AU.

**Table 3** List of the studied MCs ordered by observed time. $\Delta t$ is the crossing time of the MC in hours, $B_{\max}$ is the maximum field strength measured during that period in nT, $\Delta V_x$ it the difference of velocity between the front and back boundary from the least-square fit of Equation (32) to the data, $V_c = -\langle V_{x,\mathrm{GSE}} \rangle$, both in km s$^{-1}$. The dimensionless expansion rate, $\zeta$, is defined by Equation (32). $\sigma_\zeta$ is its standard error. The last column indicates the references where MCs have been studied previously.

| Day | Month | Year | $\Delta t$ | $B_{\max}$ | $\Delta V_x$ | $V_c$ | $\zeta$ | $\sigma_\zeta$ | Ref.[a] |
|---|---|---|---|---|---|---|---|---|---|
| 8 | 2 | 1995 | 18 | 13 | 71 | 411 | 0.98 | 0.04 | 18 |
| 4 | 3 | 1995 | 17 | 13 | 38 | 443 | 0.47 | 0.03 | 20 |
| 24 | 10 | 1995 | 10 | 10 | 34 | 373 | 0.85 | 0.15 | 8 |
| 5 | 12 | 1996 | 26 | 5 | 71 | 394 | 0.72 | 0.03 | 1 |
| 24 | 12 | 1996 | 33 | 13 | 74 | 348 | 0.78 | 0.04 | 1, 5, 21 |
| 10 | 1 | 1997 | 22 | 15 | 60 | 438 | 0.58 | 0.03 | 1, 19 |
| 7 | 11 | 1997 | 31 | 18 | 110 | 437 | 0.77 | 0.06 | 24 |
| 5 | 3 | 1998 | 35 | 13 | 83 | 348 | 0.82 | 0.04 | 4, 20 |
| 2 | 5 | 1998 | 32 | 13 | 231 | 531 | 1.06 | 0.09 | 6 |
| 2 | 6 | 1998 | 5 | 12 | 19 | 405 | 0.87 | 0.03 | 2 |
| 2 | 6 | 1998 | 8 | 12 | 29 | 398 | 0.91 | 0.05 | 20, 22 |
| 1 | 7 | 1998 | 16 | 13 | 17 | 353 | 0.35 | 0.03 | 20 |
| 19 | 8 | 1998 | 37 | 16 | 66 | 313 | 0.90 | 0.10 | 22 |
| 25 | 9 | 1998 | 32 | 19 | 204 | 649 | 0.62 | 0.04 | 12 |
| 19 | 2 | 1999 | 21 | 13 | 165 | 597 | 0.92 | 0.06 | 17 |
| 2 | 8 | 1999 | 19 | 4 | 67 | 367 | 1.10 | 0.15 | 11 |
| 15 | 9 | 1999 | 10 | 15 | 91 | 593 | 1.06 | 0.06 | 7 |
| 8 | 6 | 2000 | 26 | 15 | 184 | 630 | 0.65 | 0.09 | 15 |
| 18 | 9 | 2000 | 23 | 30 | 231 | 776 | 0.60 | 0.10 | 15 |
| 19 | 3 | 2001 | 53 | 20 | 166 | 376 | 0.92 | 0.08 | 9, 10 |
| 22 | 4 | 2001 | 25 | 15 | 56 | 360 | 0.77 | 0.03 | |
| 17 | 4 | 2002 | 32 | 14 | 126 | 469 | 0.74 | 0.04 | 13 |
| 27 | 1 | 2003 | 14 | 12 | 94 | 520 | 1.01 | 0.04 | 15 |
| 31 | 10 | 2003 | 29 | 30 | 556 | 1047 | 0.72 | 0.06 | 8, 14 |
| 9 | 11 | 2004 | 14 | 42 | 150 | 785 | 0.70 | 0.05 | 3, 16 |
| 14 | 5 | 2005 | 27 | 55 | 334 | 782 | 0.85 | 0.07 | 23 |
| | | Minimum | 5 | 4 | 17 | 313 | 0.35 | 0.03 | |
| | | Maximum | 53 | 55 | 556 | 1047 | 1.10 | 0.15 | |
| | | Mean | 23 | 17 | 128 | 505 | 0.80 | 0.06 | |
| | | Standard deviation | 11 | 11 | 115 | 177 | 0.18 | | |

[a] 1: Berdichevsky *et al.* (2002), 2: Berdichevsky, Lepping, and Farrugia (2003), 3: Dasso *et al.* (2007), 4: Du, Wang, and Hu (2007), 5: Farrugia *et al.* (2001), 6: Farrugia *et al.* (2002), 7: Hu *et al.* (2004), 8: Hu *et al.* (2005), 9: Huttunen *et al.* (2005), 10: Jian *et al.* (2006), 11: Liu *et al.* (2006), 12: Lynch *et al.* (2003), 13: Lynch *et al.* (2005), 14: Malandraki *et al.* (2005), 15: Nieves-Chinchilla, Hidalgo, and Sequeiros (2005), 16: Qiu *et al.* (2007), 17: Riley *et al.* (2003), 18: Shimazu and Vandas (2002), 19: Vandas, Romashets, and Watari (2005), 20: Watari, Watanabe, and Marubashi (2001), 21: Wei *et al.* (2003), 22: Wei *et al.* (2006), 23: Yurchyshyn *et al.* (2006), 24: Zhang *et al.* (2003).

While the spreads of $\Delta t$, $B_{\max}$, $\Delta V_x$, and $V_c$ are large, $\zeta$ is confined to a small range, with only a factor of around 3 between maximum and minimum values. Even more meaningful than extreme values, the standard deviation of $\zeta$ is less than $1/4$ of its mean, while the stan-

dard deviation of $\Delta V_x$ has a value similar to its mean. This result shows that all the analyzed MCs are basically expanding at a similar dimensionless rate when observed at 1 AU, a result not obvious from the data since $\Delta V_x$ has such a large range of values (a factor $\approx 30$). The theory developed in Section 2 allows us to disentangle the effect of the global motion and of the expansion in the observed $V_{x,\mathrm{GSE}}(t)$ to estimate the dimensionless expansion rate $\zeta$.

The result $\zeta = 0.8 \pm 0.2$ demonstrates that the MCs have similar dimensionless expansion rates even for the broad ranges of observed sizes, speeds, or field strengths. This expansion is slightly smaller than the increase of distance from the Sun when observed at 1 AU [Equation (17)]. Among the 26 MCs analyzed, only four MCs have $\zeta > 1$ so they expand slightly faster than their distance to the Sun. Of course, $\zeta$ is a combination of axial and azimuthal dimensionless expansion rates ($\zeta = l \sin^2\gamma + n\cos^2\gamma$). The determination of $l$ and $n$ needs both to estimate the MC axis orientation and to analyze the three components of the velocities. This analysis is outside the scope of present paper. However, we can compare our results with the power-laws found for the size of MCs and ICMEs in function of solar distance (see references in Section 2.5). The exponents found in the previous studies are $0.78 \pm 0.1$ and $0.61 \pm 0.09$ for MCs, and $0.92 \pm 0.07$ and 0.61 for ICMEs. So our measurement of the dimensionless expansion rate using *in situ* single spacecraft observations of the velocity, $\zeta = 0.8 \pm 0.2$, is just in between the previous results, while coming from an independent method.

## 6. Conclusion

The main aim of this work is to model the *in situ* observed velocity of interplanetary coronal mass ejections (ICMEs) and magnetic clouds (MCs) in order to derive their expansion rate. A model for the velocity is needed since only local measurements are available at a position variable with time in the ICME. Moreover, the ICME expansion has consequences on the observed magnetic field, which need to be corrected in order to have a better determination of the involved magnetic configuration.

We approach the problem by making a few hypotheses going from the most general to the most specific ones. This provides a series of equations with various levels of freedom in the functions involved. Then, the level of description (so of hypotheses) can be adapted to the available observations. We try to be as general as possible, while we also need to be predictive enough to be able to fit the model to the only temporal velocity series given by the observations. In particular, present applications to data cannot determine the shape of a free function (like the expansion function of time), so that the final equations have just free parameters. They are still general enough to incorporate an anisotropic expansion in three orthogonal directions (two being the axial and radial directions of the flux rope present in MCs).

The dynamics of an ICME is split in a global and internal one with specific hypotheses during the crossing time by the spacecraft: a constant acceleration for the global motion and a self-similar expansion for the internal motion. The predicted temporal profiles, for the observed velocities, are function of: the mean ICME velocity, $V_\mathrm{c}$ (translation velocity of the ICME center), the mean acceleration, $a$, the dimensionless expansion coefficients, $l, m, n$, the transit time from the Sun with the velocity $V_\mathrm{c}$, $\tau = D/V_\mathrm{c}$, and the angle $\gamma$ between the orientation of the flux rope axis and its global velocity.

With the order of magnitude for the physical quantities typically found in ICMEs, the model gives a nearly linear temporal dependence of the velocity, just as often observed in ICMEs. This linear temporal behavior is a combination of the global ICME motion (mainly

$V_c$) with the ICME expansion. We derive the precise contribution of both the global and expansion motions in the observed velocities [Equations (15) and (18)].

The global ICME acceleration, $a$, also implies a linear dependence of the observed velocity with time, so it needs an independent determination to separate its effect from the one coming from expansion. We estimate $a$ with three approaches: coronagraph and *in situ* observations in quadrature, a large set of ICMEs observed in a broad range of distances to the Sun, and ICMEs observed by two nearly radially aligned spacecrafts. The hypotheses and weaknesses of these approaches are different. Still, we found a coherent maximum value of the normalized mean acceleration, $|\widetilde{a}| \approx 0.1$ to 0.2. This needs to be compared to the expansion factor $\zeta \approx 0.8$. We conclude that in most ICMEs the observed velocity profile is mainly due to the expansion. This conclusion is reinforced by the results obtained previously on type II bursts, which show that the ICME deceleration is stronger close to the Sun while our above estimates give only an average deceleration along heliocentric distances (between available observations). Then, these estimates, with the three above approaches, are expected to overestimate the local acceleration, so in fact the contribution of the global ICME acceleration on the *in situ* observed velocities is expected to be lower than deduced above.

The results show that observed differences between the front and back anti-sunward velocity in ICMEs is mostly a characteristic of the expansion. However, a larger velocity difference does not necessarily imply a faster expansion! Indeed, the velocity difference between the front and the back is the product of the mean velocity, $V_c$, the ratio of ICME time duration to its transit time $\tau = D/V_c$ and the expansion coefficient $\zeta$ [Equation (33)].

As a first application of the derived equations, we have analyzed a set of 26 MCs observed by Wind or ACE spacecraft. We select MCs not affected by overtaking flows. This sample is representative of typical MCs, having typical values for the mean duration, the field strength and the global speed. Their field strength and size are distributed over a range spanning one order of magnitude. Moreover, the difference between the front and back speeds, $\Delta V_x$, has an even broader range given by a factor 30 between the minimum and maximum values. Still, within this variety of MCs, we find $\zeta = 0.8 \pm 0.2$ with the ratio of extreme values having only a factor 3. This demonstrates that, despite their broad range of $\Delta V_x$, these MCs are expanding with a similar dimensionless rate.

More generally, the derived equations give a prediction for the three components of the velocity in the flux rope and observational frames. We anticipate that the applications of these equations to MCs and ICMEs will be numerous. We give below some few applications, which we will investigate in a near future. First, the extension of these results to more cases will give a statistical base to compare the expansion of MCs and ICMEs. Second, this will allow us to investigate the possible origin of the small difference in the dimensionless expansion rate $\zeta$ found among MCs, in particular to disentangle the internal cause (like the flux rope orientation) from the effect of a variable surrounding solar wind. Finally, another direct application is the analysis of the three components of the observed velocities, in particular to determine the amount of anisotropy in the expansion.

The presence of a significant expansion has consequences on the observed magnetic fields, *i.e.*, the observed field in the front is stronger than in the back, the effect being larger for a more extended ICME (this is called the aging effect). We illustrate the effect of expansion using the Lundquist model. The comparison of the model to two MCs shows that the aging effect is not sufficient to explain the observed asymmetry in the temporal field profiles. It implies the presence of an intrinsic asymmetry in the flux rope. Future applications of the equations derived above will include the removal of the aging effect from the magnetic data using the information on the expansion coming from the observed velocity. This will allow

a better analysis, and therefore modeling, of the magnetic structure of MCs, especially for the large ones.

**Acknowledgements** The authors acknowledge financial support from CNRS (France) and CONICET (Argentina) through their cooperative science program (No. 20326). This work was partially supported by the Argentinean grants: UBACyT X329, PIP 6220 (CONICET), and PICT 03-33370 (ANPCyT). S.D. and C.H.M. are members of the Carrera del Investigador Científico, CONICET. M.S.N. is a fellow of CONICET. We are grateful to the SWE/Wind, MFI/Wind, and ACE/SWEPAM teams, for the data used for this work. P.D. thanks M.F. Landréa for clever advices on softwares.

## References

Bemporad, A., Sterling, A.C., Moore, R.L., Poletto, G.: 2005, *Astrophys. J.* **635**, L189.
Berdichevsky, D.B., Lepping, R.P., Farrugia, C.J.: 2003, *Phys. Rev. E* **67**, 036405.
Berdichevsky, D.B., Farrugia, C.J., Thompson, B.J., Lepping, R.P., Reames, D.V., Kaiser, M.L., Steinberg, J.T., Plunkett, S.P., Michels, D.J.: 2002, *Ann. Geophys.* **20**, 891.
Bothmer, V., Schwenn, R.: 1994, *Space Sci. Rev.* **70**, 215.
Burlaga, L.F.: 1988, *J. Geophys. Res.* **93**, 7217.
Burlaga, L.F.: 1995, *Interplanetary Magnetohydrodynamics*, Oxford University Press, New York.
Burlaga, L.F., Klein, L., Sheeley, N.R. Jr., Michels, D.J., Howard, R.A., Koomen, M.J., Schwenn, R., Rosenbauer, H.: 1982, *Geophys. Res. Lett.* **9**, 1317.
Cane, H.V., Richardson, I.G., Wibberenz, G.: 1997, *J. Geophys. Res.* **102**, 7075.
Chen, J.: 1996, *J. Geophys. Res.* **101**, 27499.
Cid, C., Hidalgo, M.A., Nieves-Chinchilla, T., Sequeiros, J., Viñas, A.F.: 2002, *Solar Phys.* **207**, 187.
Dasso, S., Mandrini, C.H., Démoulin, P., Farrugia, C.J.: 2003, *J. Geophys. Res.* **108**, 1362.
Dasso, S., Mandrini, C.H., Démoulin, P., Luoni, M.L.: 2006, *Astron. Astrophys.* **455**, 349.
Dasso, S., Nakwacki, M.S., Démoulin, P., Mandrini, C.H.: 2007, *Solar Phys.* **244**, 115.
Du, D., Wang, C., Hu, Q.: 2007, *J. Geophys. Res.* **112**, A09101.
Farrugia, C.J., Osherovich, V.A., Burlaga, L.F.: 1995, *J. Geophys. Res.* **100**, 12293.
Farrugia, C.J., Osherovich, V.A., Burlaga, L.F.: 1997, *Ann. Geophys.* **15**, 152.
Farrugia, C.J., Burlaga, L.F., Osherovich, V.A., Richardson, I.G., Freeman, M.P., Lepping, R.P., Lazarus, A.J.: 1993, *J. Geophys. Res.* **98**, 7621.
Farrugia, C.J., Janoo, L.A., Torbert, R.B., Quinn, J.M., Ogilvie, K.W., Lepping, R.P., *et al.*: 1999, In: Habbal, S.R., Esser, R., Hollweg, J.V., Isenberg, P.A. (eds.) *Solar Wind Nine, AIP Conf. Proc.* **471**, 745.
Farrugia, C.J., Vasquez, B., Richardson, I.G., Torbert, R.B., Burlaga, L.F., Biernat, H.K., *et al.*: 2001, *Adv. Space Res.* **28**, 759.
Foullon, C., Owen, C.J., Dasso, S., Green, L.M., Dandouras, I., Elliott, H.A., Fazakerley, A.N., Bogdanova, Y.V., Crooker, N.U.: 2007, *Solar Phys.* **244**, 139.
Farrugia, C.J., Popecki, M., Möbius, E., Jordanova, V.K., Desai, M.I., Fitzenreiter, R.J., *et al.*: 2002, *J. Geophys. Res.* **107**, 1240.
Funsten, H.O., Gosling, J.T., Riley, P., Cyr, O.C.S., Forsyth, R.J., Howard, R.A., Schwenn, R.: 1999, *J. Geophys. Res.* **104**, 6679.
Goldstein, H.: 1983, In: Neugebauer, M. (ed.) *Solar Wind Five, NASA CP-2280*, 731.
Gopalswamy, N., Hanaoka, Y., Hudson, H.S.: 2000, *Adv. Space Res.* **25**, 1851.
Gopalswamy, N., Lara, A., Yashiro, S., Kaiser, M.L., Howard, R.A.: 2001, *J. Geophys. Res.* **106**, 29207.
Gulisano, A.M., Dasso, S., Mandrini, C.H., Démoulin, P.: 2007, *Adv. Space Res.* **40**, 1881.
Harra, L.K., Crooker, N.U., Mandrini, C.H., Driel-Gesztelyi, L., Dasso, S., Wang, J., *et al.*: 2007, *Solar Phys.* **244**, 95.
Harrison, R.A., Davis, C.J., Eyles, C.J., Bewsher, D., Crothers, S.R., Davies, J.A., *et al.*: 2008, *Solar Phys.* **247**, 171.
Hidalgo, M.A., Cid, C., Vinas, A.F., Sequeiros, J.: 2002, *J. Geophys. Res.* **107**, 1002.
Hoang, S., Lacombe, C., MacDowall, R.J., Thejappa, G.: 2007, *J. Geophys. Res.* **112**, A09102.
Hu, Q., Smith, C.W., Ness, N.F., Skoug, R.M.: 2004, *J. Geophys. Res.* **109**, A03102.
Hu, Q., Smith, C.W., Ness, N.F., Skoug, R.M.: 2005, *J. Geophys. Res.* **110**, A09S03.
Hu, Q., Sonnerup, B.U.Ö.: 2001, *Geophys. Res. Lett.* **28**, 467.
Huttunen, K.E.J., Schwenn, R., Bothmer, V., Koskinen, H.E.J.: 2005, *Ann. Geophys.* **23**, 625.
Jian, L., Russell, C.T., Luhmann, J.G., Skoug, R.M.: 2006, *Solar Phys.* **239**, 393.
Klein, L.W., Burlaga, L.F.: 1982, *J. Geophys. Res.* **87**, 613.

Leitner, M., Farrugia, C.J., Möstl, C., Ogilvie, K.W., Galvin, A.B., Schwenn, R., Biernat, H.K.: 2007, *J. Geophys. Res.* **112**, A06113.
Lepping, R.P., Burlaga, L.F., Jones, J.A.: 1990, *J. Geophys. Res.* **95**, 11957.
Lindsay, G.M., Luhmann, J.G., Russell, C.T., Gosling, J.T.: 1999, *J. Geophys. Res.* **104**, 12515.
Liu, Y., Richardson, J.D., Belcher, J.W.: 2005, *Planet. Space Sci.* **53**, 3.
Liu, Y., Richardson, J.D., Belcher, J.W., Wang, C., Hu, Q., Kasper, J.C.: 2006, *J. Geophys. Res.* **111**, A12S03.
Longcope, D., Beveridge, C., Qiu, J., Ravindra, B., Barnes, G., Dasso, S.: 2007, *Solar Phys.* **244**, 45.
Lundquist, S.: 1950, *Ark. Fys.* **2**, 361.
Lynch, B.J., Zurbuchen, T.H., Fisk, L.A., Antiochos, S.K.: 2003, *J. Geophys. Res.* **108**, 1239.
Lynch, B.J., Gruesbeck, J.R., Zurbuchen, T.H., Antiochos, S.K.: 2005, *J. Geophys. Res.* **110**, A08107.
Malandraki, O.E., Lario, D., Lanzerotti, L.J., Sarris, E.T., Geranios, A., Tsiropoula, G.: 2005, *J. Geophys. Res.* **110**, A09S06.
Mandrini, C.H., Nakwacki, M., Attrill, G., Driel-Gesztelyi, L., Démoulin, P., Dasso, S., Elliot, C.H.: 2007, *Solar Phys.* **244**, 25.
Mulligan, T., Russell, C.T.: 2001, *J. Geophys. Res.* **106**, 10581.
Mulligan, T., Russell, C.T., Anderson, B.J., Lohr, D.A., Toth, B.A., Zanetti, L.J., Acuna, M.H., Lepping, R.P., Gosling, J.T., Luhmann, J.G.: 1999, In: Habbal, S.R., Esser, R., Hollweg, J.V., Isenberg, P.A. (eds.) *Solar Wind Nine, AIP Conf. Proc.* **471**, 689.
Nakwacki, M.S., Dasso, S., Mandrini, C.H., Démoulin, P.: 2008, *J. Atmos. Solar-Terr. Phys.* **70**, 1318.
Nieves-Chinchilla, T., Hidalgo, M.A., Sequeiros, J.: 2005, *Solar Phys.* **232**, 105.
Osherovich, V.A., Farrugia, C.J., Burlaga, L.F.: 1993, *J. Geophys. Res.* **98**, 13225.
Qiu, J., Hu, Q., Howard, T.A., Yurchyshyn, V.B.: 2007, *Astrophys. J.* **659**, 758.
Reiner, M.J., Kaiser, M.L., Bougeret, J.L.: 2007, *Astrophys. J.* **663**, 1369.
Reiner, M.J., Kaiser, M.L., Fainberg, J., Stone, R.G.: 1998, *J. Geophys. Res.* **103**, 29651.
Riley, P., Linker, J.A., Mikić, Z., Odstrcil, D., Zurbuchen, T.H., Lario, D., Lepping, R.P.: 2003, *J. Geophys. Res.* **108**, 1272.
Rodriguez, L., Zhukov, A.N., Dasso, S., Mandrini, C., Cremades, H., Cid, C., *et al.*: 2008, *Ann. Geophys.* **26**, 213.
Rust, D.M., Anderson, B.J., Andrews, M.D., Acuña, M.H., Russell, C.T., Schuck, P.W., Mulligan, T.: 2005, *Astrophys. J.* **621**, 524.
Schwenn, R., Lago, A., Huttunen, E., Gonzalez, W.D.: 2005, *Ann. Geophys.* **23**, 1033.
Shimazu, H., Vandas, M.: 2002, *Earth, Planets, Space* **54**, 783.
Vandas, M., Romashets, E.P.: 2002, In: Wilson, A. (ed.) *Solar Variability: From Core to Outer Frontiers, ESA SP-506*, 217.
Vandas, M., Romashets, E.P., Watari, S.: 2005, In: Fleck, B., Zurbuchen, T.H., Lacoste, H. (eds.) *Solar Wind 11 / SOHO 16, Connecting Sun and Heliosphere, ESA SP-592*, 159.1 (on CDROM).
Vršnak, B., Gopalswamy, N.: 2002, *J. Geophys. Res.* **107**, 1019.
Wang, Y., Ye, P., Zhou, G., Wang, S., Wang, S., Yan, Y., Wang, J.: 2005, *Solar Phys.* **226**, 337.
Watari, S., Watanabe, T., Marubashi, K.: 2001, *Solar Phys.* **202**, 363.
Wei, F., Liu, R., Feng, X., Zhong, D., Yang, F.: 2003, *Geophys. Res. Lett.* **30**, 2283.
Wei, F., Feng, X., Yang, F., Zhong, D.: 2006, *J. Geophys. Res.* **111**, A03102.
Weiss, L.A., Gosling, J.T., McAllister, A.H., Hundhausen, A.J., Burkepile, J.T., Phillips, J.L., Strong, K.T., Forsyth, R.J.: 1996, *Astron. Astrophys.* **316**, 384.
Wimmer-Schweingruber, R.F., Crooker, N.U., Balogh, A., Bothmer, V., Forsyth, R.J., Gazis, P., *et al.*: 2006, *Space Sci. Rev.* **123**, 177.
Yurchyshyn, V., Liu, C., Abramenko, V., Krall, J.: 2006, *Solar Phys.* **239**, 317.
Zhang, J., Dere, K.P., Howard, R.A., Bothmer, V.: 2003, *Astrophys. J.* **582**, 520.